

# Treatment of Epistemic Uncertainty in Conjunction Analysis with Dempster-Shafer Theory

L. Sanchez<sup>\*</sup> and M. Vasile<sup>†</sup>.

*Aerospace Centre of Excellence. University of Strathclyde, Glasgow, G1 1XJ, United Kingdom*

S. Sanvido<sup>‡</sup>

*Space IMS Space Consultancy GmbH, 64297, Darmstadt, Germany*

K. Mertz<sup>§</sup>

*Space Debris Office, European Space Operations Center (ESOC), European Space Agency (ESA), Darmstadt, 64293, Germany*

C. Taillan<sup>¶</sup>

*Space Security, Safety and Sustainability Office, Centre National d'Etudes Spatiales (CNES), Toulouse, 31401, France*

## Abstract

The paper presents an approach to the modelling of epistemic uncertainty in Conjunction Data Messages (CDM) and the classification of conjunction events according to the confidence in the probability of collision. The approach proposed in this paper is based on the Dempster-Shafer Theory (DSt) of evidence and starts from the assumption that the observed CDMs are drawn from a family of unknown distributions. The Dvoretzky–Kiefer–Wolfowitz (DKW) inequality is used to construct robust bounds on such a family of unknown distributions starting from a time series of CDMs. A DSt structure is then derived from the probability boxes constructed with DKW inequality. The DSt structure encapsulates the uncertainty in the CDMs at every point along the time series and allows the computation of the belief and plausibility in the realisation of a given probability of collision. The methodology proposed in this paper is tested on a number of real events and compared against existing practices in the European and French Space Agencies.

## Acronyms

**Bel** Belief

**bpa** basic probability assignment

**CAM** Collision Avoidance Manoeuvre

**CARA** Conjunction Assessment Risk Analysis

<sup>\*</sup>PhD Candidate, Aerospace Centre of Excellence, luis.sanchez-fdez-mellado@strath.ac.uk.

<sup>†</sup>Professor at University of Strathclyde and Director of Aerospace Centre of Excellence, massimiliano.vasile@strath.ac.uk, AIAA Associate Fellow. Corresponding author.

<sup>‡</sup>Space Debris Engineer. IMS Space Consultancy GmbH, silvia.sanvido@ext.esa.int.

<sup>§</sup>Spaces Debris Engineer, Space Debris Office, ESA/ESOC, klaus.merz@esa.int.

<sup>¶</sup>Space Surveillance Engineer. Space Security, Safety and Sustainability Office, CNES, christophe.taillan@cnes.fr.

**CDF** Cumulative Distribution Function

**CDM** Conjunction Data Message

**CNES** Centre National d'Etudes Spatiales

**DKW** Dvoretzky–Kiefer–Wolfowitz

**DSt** Dempster-Shafer theory of evidence

**eCDF** empirical Cumulative Distribution Function

**ESA** European Space Agency

**ESOC** European Space Operations Centre

**FE** Focal Element

**FN** False Negative

**FP** False Positive

**HBR** Hard-Body Radius

**JAC** Java for Assessment of Conjunctions

**KS** Kolmogorov-Smirnov

**LEO** Low Earth Orbit

***Pl*** Plausibility

**PoC** Probability of Collision

**SDO** Space Debris Office

**sPoC** scaled Probability of Collision

**TCA** Time of Closest Approach

**TP** True Positive

## I. Introduction

The close encounter of two space objects, also known as a conjunction between a chaser and a target, can lead to a collision if the relative position of the two objects is not properly controlled. The Probability of Collision (PoC) to happen depends on the probability that each of the two objects occupies a given position in space. This probability can be derived from the knowledge of the orbit of the two objects and the associated uncertainty.

It is customary to assume that the distribution of possible positions of the two objects at the time of closest encounter follows a multivariate Gaussian with a given mean and covariance matrix[1, 2]. This assumption is limited by three

sources of uncertainty: the uncertainty in the dynamic model used to propagate the orbit from the last available observation to the time of closest approach, the uncertainty in the actual distribution at the time of closest approach, and the uncertainty in the last observed state before closest approach. We argue that all three forms of uncertainty are epistemic in nature since they derive from a lack of knowledge of the model, distribution and error in the observations.

The information on a given close encounter is generally available in the form of a Conjunction Data Message (CDM), which contains the means and covariances of the two objects at Time of Closest Approach (TCA)[3]. Thus, in this paper, we start from the assumption that the mean and covariance in each CDM are affected by epistemic uncertainty, which is reflected in an uncertainty in the correct value of the PoC.

The general attempt to compensate for the uncertainty in the CDMs is to improve the realism of the covariance matrix by improving its propagation[4] or by some form of updating of the dynamic model[5]. These approaches are all very valuable but require direct access to the post-observation data. Other methods based solely on the available CDMs tried to predict the next CDMs using machine learning starting from an available time series[6–9] or increased the last covariance under the assumption that the series of CDMs should follow a given distribution [10, 11]. This last approach does not modify the mean value or miss distance.

So far, only a limited number of authors have directly addressed epistemic uncertainty in conjunction analysis [12–15]. In [16–18] the authors proposed a robust approach to conjunction analysis and collision avoidance planning based on Dempster-Shafer theory of evidence (DSt). DSt allows making decisions informed by the degree of confidence in the correctness of a value rather than by the value itself [19]. However, the available information to build the frame of discernment that is needed in DSt is often limited in a sequence of CDMs. CDMs contain little information on the three forms of uncertainty listed above and essentially only provide covariance and miss distance. Thus, one key question is how to translate the time series of CDMs into the frame of discernment used in DSt. The underlying assumption in this work is that the CDMs are observables drawn from an unknown family of distributions defined within some bounds. Without uncertainty, one would be able to exactly predict the next CDMs as the mean and covariance would only depend on observations with a known distribution and there would be no uncertainty in the propagation model and distribution at TCA. Furthermore, we assumed that the CDMs computed from observations acquired close to the TCA were less affected by model and distribution uncertainty. This is reasonable as the propagation time is shorter and thus both nonlinearities and model errors have a lower impact on the propagation of the distribution of the possible states.

The paper introduces a methodology, based on the Dvoretzky–Kiefer–Wolfowitz (DKW) inequality[20], to derive a DSt structure capturing the epistemic uncertainty in a given sequence of CDMs. From the DSt structures, one can compute the Belief (*Bel*) and Plausibility (*Pl*) that the value of the PoC is correct and an upper and lower bound on its value. The paper then proposes a classification system that exploits the use of *Bel* and *Pl* to differentiate between events that are uncertain from events that can lead to a collision. The overall methodology is tested on a number of synthetic and real conjunction scenarios with known sequences of CDMs and compared against current practices in the European

Space Agency (ESA) and Centre National d'Etudes Spatiales (CNES).

The rest of the paper is structured as follows. Section II briefly introduces a methodology previously presented by the authors to deal with epistemic uncertainty for risk assessment in space encounters. Section III extends this methodology to deal with sequence of CDMs. In Section IV, some numerical cases are presented showing the operation of the proposed method and comparing the approach with the procedure followed by real operators. Finally, Section V concludes the paper with the final remarks and future work.

## II. Conjunction Analysis with Dempster-Shafer Structures

This section briefly introduces the basic idea of DSt applied to Conjunction Assessment Risk Analysis (CARA). It also includes the DSt-based conjunction classification system already introduced by the authors in previous works. More details on DSt can be found in [21], and more details on its application to space conjunction assessment can be found in [16–18].

In this paper, we consider only fast encounters between two objects: object 1 and object 2. Under the typical modelling assumptions of fast encounters [22], the PoC can be defined as:

$$PoC = \frac{1}{2\pi\sqrt{|\Sigma|}} \int_{\mathcal{B}((0,0),R)} e^{-\frac{1}{2}((\mathbf{b}-\boldsymbol{\mu})^T \Sigma^{-1} (\mathbf{b}-\boldsymbol{\mu}))} d\xi d\zeta \quad (1)$$

where, without loss of generality, object 2 is at the centre of the coordinate system of the impact plane at the time of closest approach (TCA),  $\mathbf{b} = [\xi, \zeta]^T$  is the position vector of object 1 with respect to object 2 projected onto the impact plane,  $\Sigma$  is the  $2 \times 2$  combined covariance matrix of the position of the two objects in the impact plane ( $\Sigma = \Sigma_1 + \Sigma_2$ , with  $\Sigma_1$  and  $\Sigma_2$  the individual covariance matrices of object 1 and 2 respectively) and  $\boldsymbol{\mu} = [\mu_\xi, \mu_\zeta]^T$  is the expected position vector of object 1 with respect to object 2 projected onto the impact plane. The integration region  $\mathcal{B}((0,0),R)$ , or Hard-Body Radius (HBR), is a disk with radius  $R$  centred at the origin of the impact plane.

When the covariance  $\Sigma$  and miss distance  $\boldsymbol{\mu}$  are not precisely known the  $PoC$  is affected by a degree of uncertainty. This lack of knowledge translates into an epistemic uncertainty in the exact value of  $\Sigma$  and  $\boldsymbol{\mu}$ . The epistemic uncertainty in covariance  $\Sigma$  and miss distance  $\boldsymbol{\mu}$  can come from incertitude in the sources of information, from poor knowledge of the measurements or propagation model or from an approximation of the actual distribution on the impact plane at TCA. As shown in [16] and [17], this epistemic uncertainty can be modelled with DSt.

The idea proposed in [16], was to use DSt to compute the level of confidence in the correctness of the value of the PoC, given the available evidence on the sources of information. Each component of the combined covariance matrix in the impact plane,  $[\sigma_\xi^2, \sigma_\zeta^2, \sigma_{\xi\zeta}]$ , was modelled with one or more intervals and so was the miss distance  $[\mu_\xi, \mu_\zeta]$ . A basic probability assignment (*bpa*) was then associated with each interval. The intervals and the associated *bpa* can be derived, for example, directly from the raw observations [15, 23] or from a time series of CDMs [3] as explained later in

this paper.

Given the intervals and associated *bpa*, one can compute the cross-product of all the intervals under the assumption of epistemic independence. Each product of intervals with non-zero *bpa* constitutes a Focal Element (FE),  $\gamma_i$ , whose joint *bpa* is the product of the *bpas* of the individual intervals. When computing the PoC, each FE defines a family of bi-variate Gaussian distributions on the impact plane. In the following, the collection of all focal elements forms the uncertainty space  $U$ , and the uncertain parameter vector is  $\mathbf{u} = [\mu_\xi, \mu_\zeta, \sigma_\xi^2, \sigma_\zeta^2, \sigma_{\xi\zeta}]^T$  so that  $\mathbf{u} \in U$ .

Given the sets  $\Phi = \{PoC | PoC \geq PoC_0\}$  and  $\Omega = \{\mathbf{u} \in U | PoC(\mathbf{u}) \in \Phi\}$  the *Pl* and *Bel* that the *PoC* is larger than a given threshold  $PoC_0$  given the available evidence are:

$$Bel(\Omega) = \sum_{\gamma_i \subset \Omega} bpa(\gamma_i) \quad (2a)$$

$$Pl(\Omega) = \sum_{\gamma_i \cap \Omega \neq \emptyset} bpa(\gamma_i) \quad (2b)$$

For different values  $PoC_0$ , Eqs. (2a) and (2b) define two curves (see the example in Fig. 1). The area between the curves,  $A_{Pl,Bel}$ , in logarithmic scale, is:

$$A_{Pl,Bel} = \int_{\log(PoC)}^0 Pl(\Omega) d(\log(PoC)) - \int_{\log(PoC)}^0 Bel(\Omega) d(\log(PoC)) \quad (3)$$

$Bel(\Omega)$  is a lower bound on the probability that  $PoC \geq PoC_0$ . Its value is computed by adding up all the FEs fully supporting the hypothesis  $PoC \geq PoC_0$ .  $Pl(\Omega)$  is an upper bound on the probability that  $PoC \geq PoC_0$ . Its value is computed by adding up all the FEs only partially supporting the hypothesis  $PoC \geq PoC_0$ . The area  $A_{Pl,Bel}$  quantifies the amount of uncertainty on the probability that  $PoC \geq PoC_0$ , i.e. if no epistemic uncertainty is present, both curves would reduced to the same Cumulative Distribution Function (CDF). Thus, for a given value of  $PoC_0$ , a large value of  $Pl$  associated with a small value of  $A_{Pl,Bel}$  suggests that there is a lot of support to the hypothesis  $PoC \geq PoC_0$  given the available information. On the contrary a large value of  $Pl$  associated to a large value of  $A_{Pl,Bel}$  suggests that the hypothesis  $PoC \geq PoC_0$  is very plausible to be true but with a high degree of uncertainty.

In [16], a DSt-based classification system was proposed to decide whether, for a given conjunction event, a Collision Avoidance Manoeuvre (CAM) was required or not. In this paper, we propose a revised version of the classification approach proposed [16]. A given conjunction event is classified according to: i) the value of the *Pl* at  $PoC = PoC_0$  or  $Pl(PoC_0)$ , ii) the time of closest approach *t2TCA* and iii) the area  $A_{Pl,Bel}$ . We introduced five thresholds: two time thresholds indicating the proximity of the event,  $T_1$  and  $T_2$ , the maximum admissible *PoC*, or  $PoC_0$ , the level of *Pl*,  $Pl_0$ , above which there is sufficient support to the hypothesis  $PoC \geq PoC_0$ , and the value of  $A_{Pl,Bel}$ ,  $A_0$ , above which the information is considered to be uncertain. Three of the five thresholds,  $T_1$ ,  $T_2$  and  $PoC_0$ , are decided by the operators

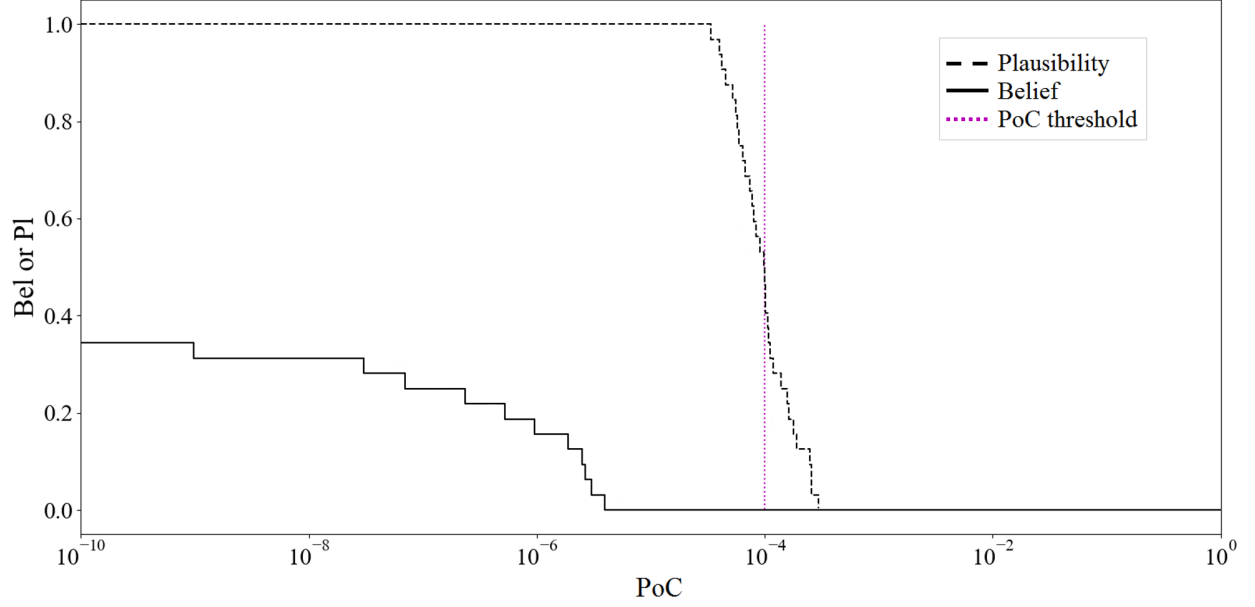


**Fig. 1** Support to the value of  $PoC$  being greater than a given value:  $Bel$  -black solid line;  $Pl$  - black dashed line. The dotted purple line represents a possible  $PoC_0$ .

and depend on operational constraints, the other two  $Pl_0$  and  $A_0$  need to be tuned on a large body of encounter scenarios, as it will be explained in the remainder of the paper.

We then introduce the following six classes, see Table 1, each defined by a combination of  $Pl(PoC_0)$ ,  $t2TCA$  and  $A_{Pl,Bel}$ :

**Table 1** Conjunction risk assessment evidence-based classification criterion.

Time to TCA	Pl at $PoC_0$	Area between curves	Class
$t2TCA \leq T_1$	$Pl(PoC_0) < Pl_0$	-	5
	$Pl(PoC_0) \geq Pl_0$	$A_{Pl,Bel} < A_0$	1
		$A_{Pl,Bel} \geq A_0$	0
$T_1 < t2TCA$ $t2TCA \leq T_2$	$Pl(PoC_0) < Pl_0$	-	4
	$Pl(PoC_0) \geq Pl_0$	$A_{Pl,Bel} < A_0$	2
		$A_{Pl,Bel} \geq A_0$	3
$t2TCA > T_2$	-	-	3

- *Class 0*: there is enough evidence supporting  $PoC \geq PoC_0$  but is accompanied by a high degree of uncertainty and no time to acquire new measurements, due to the proximity of the event, hence a CAM is recommended.
- *Class 1*: there is full support to the hypothesis  $PoC \geq PoC_0$ , with limited uncertainty, and short  $t2TCA$ , hence a CAM is required.

- *Class 2*: there is full support to the hypothesis  $PoC \geq PoC_0$ , with limited uncertainty, preparing a CAM is recommended, but a CAM is not executed yet due to the available time before the encounter.
- *Class 3*: there is enough evidence supporting  $PoC \geq PoC_0$  but is accompanied by a high degree of uncertainty with sufficient time to acquire new measurements, hence more measurements should be acquired.
- *Class 4*: there is insufficient evidence supporting  $PoC \geq PoC_0$  and sufficient time to acquire new measurements.
- *Class 5*: no action is implemented, since  $t2TCA$  is too short and there is insufficient evidence supporting  $PoC \geq PoC_0$ .

Note that for  $t2TCA > T_2$  all events are classified as Class 3 because the required action is to acquire more measurements. Also, it has to be noted that the level of confidence that one has in the computed value of the  $PoC$  depends only on  $Pl_0$ . If  $Pl_0$  is set to zero it means that one accepts even a single piece of partial evidence that  $PoC \geq PoC_0$  to escalate the Class from 5, to 0 or 1, or from 4 to 2 or 3.

### III. Modelling Epistemic Uncertainty in Conjunction Data Messages

The use of DSt to model epistemic uncertainty does not require any assumption on the probability of an event and also captures rare events with low probability. On the other hand with no direct information on measurements and dynamic model, one can only rely on the CDMs to define the FEs and associated probability masses.

This section presents a methodology to associate one of the six classes introduced in the previous section to a given sequence of CDMs. The first step is to derive the FEs from the time series of miss distances and covariance matrices in the CDMs. In accordance with DSt, we make no prior assumption on the underlying distribution of the CDMs and, instead, we consider that each CDM is drawn from an unknown set of probability distributions. The assumption is that the value of the uncertain vector  $\mathbf{u}$  in each CDMs is a sample drawn from the set of unknown distributions. We make use of the DKW inequality[20], to build an upper and lower bound to the set starting from the empirical Cumulative Distribution Function (eCDF) derived from the sequence of CDMs.

Given a sequence of CDMs and the eCDF of each of the components of the uncertain vector  $\mathbf{u}$  the DKW inequality, defines the following upper and a lower bounds

$$F_n(x) - \sqrt{\frac{\ln \frac{2}{\delta}}{2n}} \leq \mathcal{F}(x) \leq F_n(x) + \sqrt{\frac{\ln \frac{2}{\delta}}{2n}} \quad (4)$$

around the eCDF  $F_n(x)$  (dashed green lines in Fig. 2b), given  $n$  CDMs and the confidence level  $1 - \delta$  that the exact distribution  $\mathcal{F}(x) \in F_n(x) \pm \varepsilon$ , where  $\varepsilon = \sqrt{\frac{\ln \frac{2}{\delta}}{2n}}$ .

From the confidence region defined by the DKW bands, it is possible to build a probability box, or p-box [24–26], for each of the components of  $\mathbf{u}$ . A p-box is a set of all CDFs compatible with the data, that is, the bounded region containing all distributions from where the set of samples may have been drawn [25]. The upper and lower bounds of

the p-box are monotonic non-decreasing functions, ranging from 0 and 1, so that  $\underline{\mathcal{F}}(x) \leq \mathcal{F}(x) \leq \overline{\mathcal{F}}(x)$ , with  $\underline{\mathcal{F}}(x)$  and  $\overline{\mathcal{F}}(x)$  the upper and lower bounds of the p-box for a given variable  $x$  [24].

In this work, the p-box bounds are computed from the CDF of a weighted sum of univariate Gaussians, each one centred at one of the samples. More formally the assumption is that  $\mathcal{F}(x)$  can be approximated by:

$$\mathcal{F}(x) \sim \mathcal{P}(x) = \int_{-\inf}^{\inf} \sum_i^n w_i \mathcal{N}(x_i, \sigma_i; x) dx, \quad (5)$$

with  $x_i$  the realisations of the uncertain variable  $x$ ,  $w_i$  a weight associated with each sample, and  $\sigma_i$  the variance of the Gaussian distribution associated with the  $i$ th-sample. See Fig. 2a for an illustrative example. Implicitly, it implies that each sample presents some uncertainty which is modelled with a Gaussian distribution (grey lines in Fig. 2a). This distribution represents the confidence in the sample's value.

In order to define the p-box's limits, the two free parameters on each Gaussian distribution on the weighted sum,  $w_i$  and  $\sigma_i$ , must be computed by solving the optimisation problems:

$$\begin{cases} \overline{\mathcal{P}}(x) = \max_{w_i, \sigma_i} \mathcal{P}(x; w_i, \sigma_i) \\ \underline{\mathcal{P}}(x) = \min_{w_i, \sigma_i} \mathcal{P}(x; w_i, \sigma_i) \end{cases} \quad s.t. \quad \begin{cases} \overline{\mathcal{P}}(x) \leq \min(1, F_n(x) + \epsilon) \\ \underline{\mathcal{P}}(x) \geq \max(0, F_n(x) - \epsilon) \end{cases}, \quad (6)$$

where  $\overline{\mathcal{P}}(x)$ ,  $\underline{\mathcal{P}}(x)$  are the upper and lower bounds of the p-box, respectively (red dashed-pointed line in Fig. 2c). An approximation to  $\overline{\mathcal{P}}(x)$ ,  $\underline{\mathcal{P}}(x)$  can be computed by finding the values of  $w_i$  and  $\sigma_i$  in Eq. (5) that best fit the upper and lower DKW bands:

$$\begin{cases} \overline{\mathcal{P}}(x) \approx \overline{P}(x) = \text{fit}_{w_i, \sigma_i}(F_n(x) + \epsilon) \\ \underline{\mathcal{P}}(x) \approx \underline{P}(x) = \text{fit}_{w_i, \sigma_i}(F_n(x) - \epsilon) \end{cases} \quad (7)$$

Eq. (7) gives the upper and lower bounds on the probability of realising a particular value of the uncertain vector  $\mathbf{u}$  but the definition of a set of intervals for each component of  $\mathbf{u}$  requires first the definition of the range of each component. Eq. (5) suggests that each p-box has infinite support. However, this would lead to an inconvenient infinite range for variance and miss distance. Instead, in the following we define the more practical interval  $[\underline{x}, \overline{x}]$  such that:

$$\int_{\underline{x}}^{\infty} w_1 \mathcal{N}(x_1, \sigma_1; x) dx = 0.99, \quad \int_{-\infty}^{\overline{x}} w_n \mathcal{N}(x_n, \sigma_n; x) dx = 0.99, \quad (8)$$

It is important to note that the assumption is that the miss distance and each component of the covariance can be treated independently. This is generally not the case, however, the independence assumption in this paper leads to a more conservative set of focal elements that cover the space of realisations of the uncertainty vector. Although this can lead to over-conservative decisions, it is deemed to be acceptable in the case of high-risk events with little available



information.

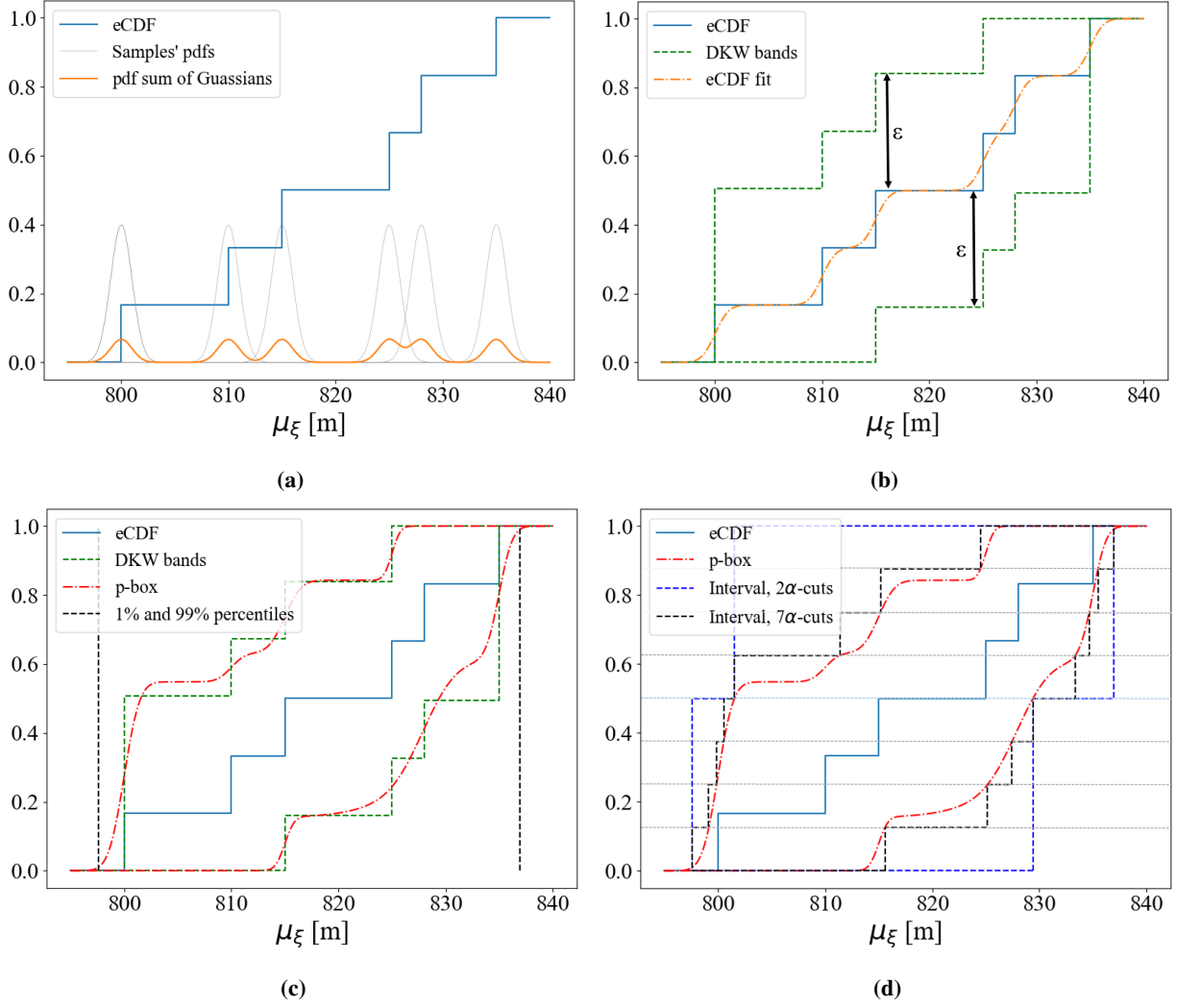


**Fig. 2** Example of intervals derivation form the eCDF. (a) eCDF (solid blue), individual sample's Gaussian pdf distributions (solid grey), pdf of the sum of Gaussian distributions for the eCDF fit (solid orange) (b) eCDF (solid blue), DKW bands (dashed green), fitted eCDF with weighted sum of Gaussian distributions (dashed-pointed orange). (c) eCDF (solid blue), DKW bands (dashed green), p-box optimising the weighted sum of Gaussian distributions (dashed-pointed red), 1% and 99% percentiles (vertical pointed black lines). (d) eCDF (solid blue), p-box (dashed-pointed red), 1  $\alpha$ -cut 2 intervals' PI and Bel (dashed blue), 7  $\alpha$ -cuts 8 intervals' PI and Bel (dashed black). Dotted thin horizontal lines for the  $\alpha$ -cuts: light blue at 0.5 for the 2 intervals partition, grey lines spaced 0.125 for the 8 intervals partition.

### A. Scaling of the CDMs

The approach described in previous sections assumes that every CDM has the same relative importance and no additional source of information is available to qualify each individual CDM. However, as the  $r2TCA$  decreases, so does the effect of the uncertainty on the true shape of the distribution on the impact plane and the effect of model uncertainty in the propagation. Fig. 3a shows the normalised determinant of multiple sequences of covariance matrices

taken from the database of the ESA's Collision Avoidance Kelvins Challenge [8, 27]. The database contains 13,152 sequences of CDMs of some of the Low Earth Orbit (LEO) satellites monitored by the ESA Space Debris Office (SDO). The figure shows that one can fit the simple exponential law  $y' = e^{-3t'}$  to the magnitude of the determinant (red line in the figure). However, one cannot simply trust later CDMs due to large uncertainty in each individual sequence. Thus, we propose the following fit for each individual sequence:

$$y' = Ce^{At'} + B \quad A, B, C \geq 0, \quad (9a)$$

$$y' = \frac{\|\Sigma\|}{\max_{CDMs}(\|\Sigma\|)} \quad (9b)$$

$$t' = \frac{(1 - \max_{CDMs}(t2TCA))}{(\min_{CDMs}(t2TCA) - \max_{CDMs}t2TCA)} \quad (9c)$$

Once the parameters  $A, B$  and  $C$  are fitted to the samples from a given sequence, the following weight is associated with each CDM in that sequence:

$$w_{CDM_i} = \frac{1}{y'(t2TCA_{CDM_i})} \quad (10)$$

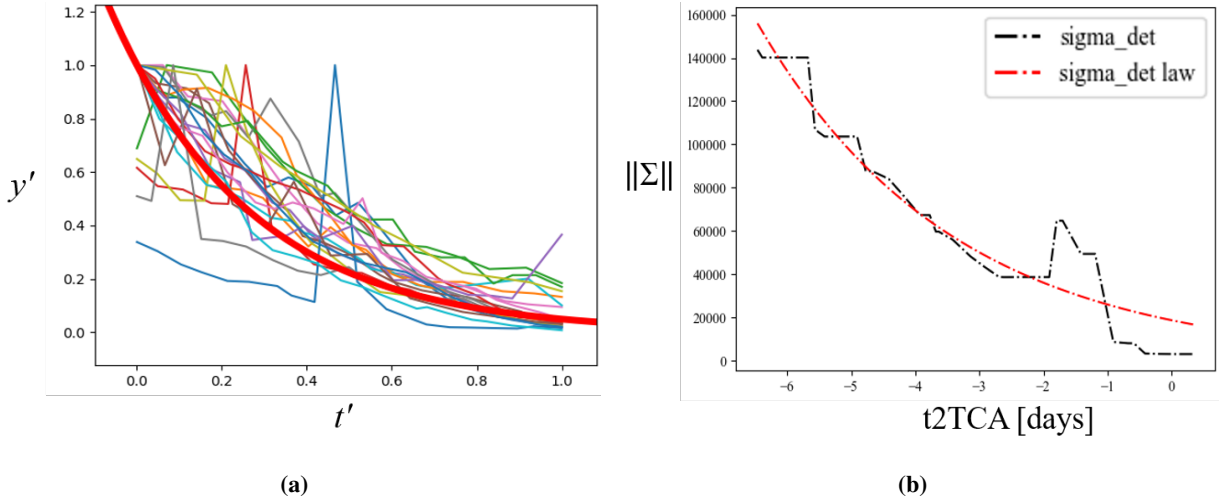


**Fig. 3** Fitting law: (a)  $y' = e^{-3t'}$  (thick red line) and the dimensionless covariance determinant for a number of sequences of CDMs (thinner lines), (b) Fitted law (dashed-pointed red) of a single CDM sequence (dashed-pointed black).

This approach results into a scaling of the probability mass associated with the CDMs but still allows the quantification of highly uncertain CDMs since there is no filtering process. The reason is that, with no information on trusted sources or individual CDMs, one cannot make any assumption on which CDM is more credible.

## B. $\alpha$ -cuts and DSt Structures

Once the p-box is defined, the intervals for each component of  $\mathbf{u}$  are derived from a series of equally spaced  $\alpha$ -cuts, light blue and grey dotted horizontal thin lines in Fig. 2d. Each  $\alpha$ -cut creates interval[28, 29]:

$$[x_\alpha, x^\alpha] = \{x \mid \mathcal{F}(x) \geq \alpha\}. \quad (11)$$

The intersection with the upper bounds in the p-box defines the lower limit of the interval, and the intersections with the lower bound define the upper limit of the interval. The number of intervals is equal to the number of cuts plus one, and the *bpa* associated with each interval, assuming the cuts are evenly spaced, is equal to the inverse of the number of cuts. The intervals and their *bpa* will define an envelope around the p-box (blue and black dashed lines in Fig. 2d). The greater the number of  $\alpha$ -cuts, the closer the envelope will be to the p-box, but the more computationally expensive is the computation of *Bel* and *Pl*. From the intervals associated with each component of  $\mathbf{u}$  the *Pl*, *Bel* of  $PoC \geq PoC_0$  are computed with Eq. (2) (see Fig. 4) and the conjunction event is classified according to Table 1.

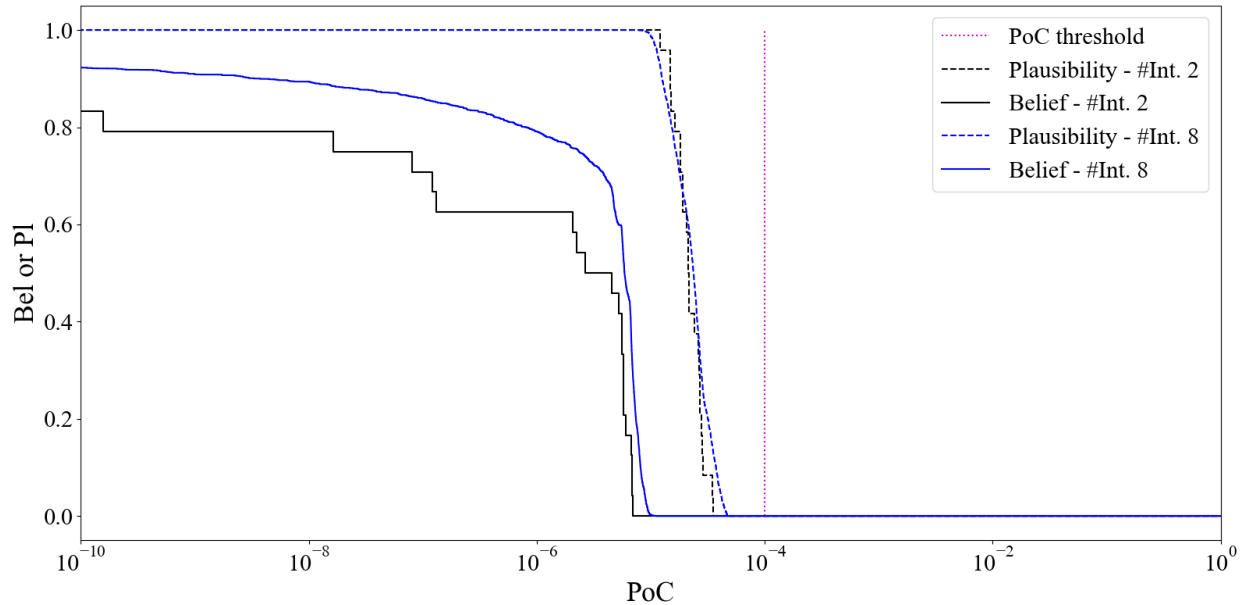


**Fig. 4** Plausibility and Belief of  $PoC \geq PoC_0$ . Black: 1  $\alpha$ -cut (two intervals) per variable, 32 FEs. Blue: 7  $\alpha$ -cut (eight intervals) per variable, 32768 FEs. Solid lines: belief. Dashed lines: plausibility. Dotted purple vertical line:  $PoC_0$ .

Even in this case, we maintained the assumption that variables are independent. Approaches to address dependencies already exist in the literature [30] and will be considered in future works. The independence assumption has two implications: i) the uncertainty space  $U$  is an outer approximation of the space of all distributions of  $\mathbf{u}$  and ii) some focal elements might not contain any sample of  $\mathbf{u}$ . The combination of the two generally leads to over-conservative results. Thus, in order to have less conservative results, yet coherent with DSt, a *bpa* = 0 is assigned to all empty FEs

and their  $bpa$ , coming from the Cartesian product, is evenly distributed to the rest of FEs so that  $\sum_i bpa_i = 1$ .

## IV. Numerical experiments

In this section, a number of numerical tests are presented. The aim is to show the applicability of the methodology presented in previous sections and compare its outcome to the decisions made in past real cases by actual satellite operators: European Space Operations Centre (ESOC) and CNES.

### A. Robust conjunction assessment on virtual conjunctions

This example shows the operations of the method applied to a synthetic database, as a previous step before applying the method to real cases. This example shows the applicability of the approach and the capacity of the system to differentiate between high-risk and low-risk scenarios, but also to catalogue events as uncertainty if information is poor or contains contradictory evidence. The advantage of using a synthetic database is the fact the outcome of the event is known: collision or no collision, so it can be analysed the number of correctly classified events, and more importantly, the fraction of events catalogued in the uncertain classes.

#### 1. Synthetic database

To create the database, a number of close encounters and associated CDMs were simulated. First, the true primary's positions and the actual miss distance at the TCA epoch were obtained. The position was randomly selected from:  $a \in [6850, 7200]\text{km}$ ,  $e \in [10^{-20}, 10^{-6}]$ ,  $i \in [0, 90]\text{deg}$ ,  $\Omega \in [0, 360]\text{deg}$ ,  $\omega \in [0, 360]\text{deg}$ ,  $\theta \in [0, 360]\text{deg}$ ; and the miss distance was drawn from a log-normal distribution with  $\mu_{\lognorm} = 3\text{m}$  and  $\sigma_{\lognorm} = 1\text{m}$ , so that one could ensure that there was a sufficient number of collision cases. Along with the miss distance, the physical properties of the satellites were selected, being the HBR the most relevant for the analysis. An encounter is classified as a collision when the miss distance is smaller than the HBR, which is computed as the sum of the individual object's radius randomly drawn from the intervals  $HBR_1 \in [1, 10]\text{m}$  and  $HBR_2 \in [0.5, 1.5]\text{m}$ . The secondary object's position is obtained from the relative distance and the primary's positions, and the velocity is obtained by randomly rotating the velocity vector, ensuring the object's orbit falls within the above bounds.

The nominal orbits are back propagated from the encounter epoch (randomly selected along the year 2023) to the first observation epoch, which may vary from 1.5 to 7 days. The next step is to add uncertainty to the position of both objects at this first observation epoch. The uncertainty in the state estimation at the first observation epoch is assumed to follow a Gaussian distribution, with a mean equal to the nominal orbit and a diagonal covariance matrix in the object's  $\langle R, T, H \rangle$  reference frame whose terms are randomly drawn from:  $\sigma_{rr} \in [50, 75]\text{m}$ ,  $\sigma_{tt} \in [250, 300]\text{m}$ ,  $\sigma_{hh} \in [50, 75]\text{m}$ . The error on the first observation is, different for each object.

A random number of observations, between 6 and 15 for each object, and the associated epoch, randomly distributed

between the initial and the encounter epochs, are generated for each sequence of synthetic CDMs. Each time a new observation, for any of the two objects is simulated, a new error associated with the observation is assigned to the state of the object. All observation errors follow a Gaussian distribution, with the same mean and covariance of the first observation. From each observation, the uncertainty is propagated to the TCA by sampling the ellipsoids and propagating the samples. Once at the encounter epoch, the relative state vectors, combined covariance matrix, PoC and other relevant quantities are computed, creating the virtual CDM of the encounter associated with the latest observation. This approach makes the same assumption considered when generating real CDMs: regardless of the actual distribution of the samples at TCA, the CDM is generated by computing the mean and covariance of the samples.

A total of 500 encounters, summing up to a total of 7,587 CDMs, were created. Around 10% were Collision scenarios and the rest Non-Collision encounters. We opted to keep a higher proportion of non-collision encounters, as it is usually the case for databases of real CDMs, although with a higher proportion of high-risk events to have enough representative cases.

## 2. Thresholds

In order to assess the risk of the encounters, the thresholds involved in Table 1 have to be defined. The time thresholds and the risk threshold are set according to the example in the next sections:  $T_1 = 3$  days,  $T_2 = 5$  days,  $PoC_0 = 10^{-4}$ . These thresholds are usually defined statistically based on the collision rate tolerated by the satellite and are usually mission and operator-dependent. The other two thresholds are related to the epistemic framework, so current operation approaches do not have a methodology to set their value.

In order to carry out the analysis, the value of the epistemic thresholds is been selected trying to avoid the False Negatives (FNs) (collision cases classified as low-risk), and reducing the False Positives (FPs) (no collision cases miss-classified as high-risk) while maximising the proportion of True Positives (TPs) (collision cases correctly classified). From the criterion in Table 1, the support threshold,  $Pl_0$ , influences exclusively the classification of the low-risk events, while the confidence threshold  $A_{Pl,Bel}$  affects determine which of the remaining cases are classified as high-risk or uncertain. Thus, both thresholds are not couples and can be selected independently.

According to the classification in Table 1, the expected outcome is that low values of  $Pl_0$  would increase the number of events classified as Class 1 or 2, increasing the possibility of maximising the amount of TPs, if this is combined with high values of  $A_{Pl,Bel}$ , the chances of detecting all high-risk events is high, but at the cost of increasing the number of FPs. If  $A_{Pl,Bel}$  is low, instead, more events classified as uncertain (Class 0 and 3) will appear. On the contrary, a higher value of  $Pl_0$  would reduce the false alerts, but would increase the number of FNs.

In order to avoid FNs, the value of  $Pl_0$  should be low. Thus, the value has been selected so that if there is some support for higher values of PoC, then the event pass to the next filter. This means that there will be enough support if at least on FE with  $\max(PoC) > PoC_0$ , which sets the value of the threshold equal to  $Pl_0 = 1/\#FE$ . For the support

threshold, we argue that the decision to execute a CAM is thus related to the confidence of the operator in the quality of the CDM. For highly uncertain CDM a low  $A_{Pl,Bel}$  is recommended but if the quality of the CDM is high a higher  $A_{Pl,Bel}$  should be used. To avoid the increase on FPs, a lower value is selected. The threshold is selected according to the fraction of the maximum possible area between the curves. The area between the curves is measured using the logarithmic scale in the PoC axis, thus a minimum value  $\underline{PoC}$  should be selected. In this paper  $\underline{PoC} = 10^{-30}$  since it is the lowest value appearing in the CDMs. That maximum area between the curves,  $A_{max}$  corresponds when the  $Bel$  decrease from 1 to 0 at  $\underline{PoC}$  and the  $Pl$  at  $PoC = 1$ , corresponding to the maximum uncertainty scenario. Thus, the confidence threshold on the rest of the paper is given as  $A_{Pl,Bel} = A_{max} \cdot A_{Pl,Bel}^*$ . For the example of this section and in the following examples,  $A_{Pl,Bel} = 0.1$ ,  $A_{max} = 30$  and  $A_{Pl,Bel}^* = 3$ .

**Table 2** Threshold values.

Threshold	Units	Value
$T_1$	days	3
$T_2$	days	5
$PoC_0$	-	$10^{-4}$
$Pl_0$	-	$1/\#FE$
$A_{Pl,Bel}$	-	3
$\underline{PoC}$	-	$10^{-30}$
$A_{Pl,Bel}^*$	-	0.2

### 3. Results on synthetic database

For all the 500 encounters, each sequence of CDMs was assessed every time a new CDM was generated, resulting in a total of 7,587 sequence evaluations.

Note, that according to the classification criteria, if  $Pl_0 = A_{Pl,Bel} = 0$ , no event can be classified as high-risk (thus  $\#TP = \#FP = 0$ ), but no actual Collision event should be classified as low-risk (thus,  $\#FN = 0$ ) either. In this case, we can check that the virtual CDMs in the synthetic database are actually randomly generated without any bias. As can be seen in Fig. 5, for  $Pl_0 = A_{Pl,Bel} = 0$ , no FN is detected, as expected.

Coming back to the selected threshold, Fig. 6, shows the Confusion matrix with the set of thresholds in Table 2.

The figure shows that there are no collision cases that are incorrectly classified as non-collisions. On the other hand, the degree of uncertainty leads a number of cases to be classified as Class 1 and 2 although no collision occurs. A reduction of the value of  $A_{Pl,Bel}^*$  would transfer most of these cases into Class 0 or 3 but at the same time, a number of true collisions would also be classified as Class 0 or 3, the uncertain classes, because they are indistinguishable from a non-collision case. As it will be shown in the remainder of the paper, the level of ambiguity in the real database of CDMs appears to be lower than in the synthetic database to the point that even in the case of substantial uncertainty in

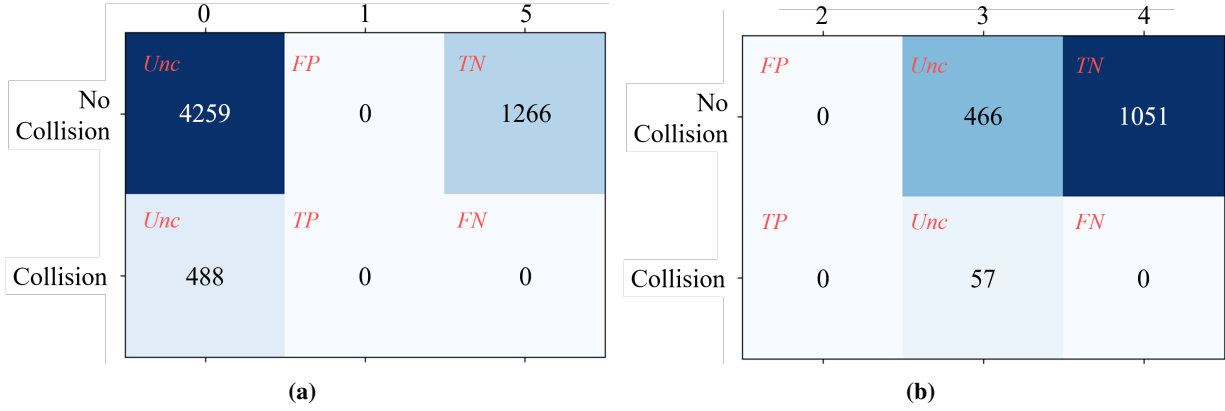


**Fig. 5** Number of TP, TN, FP, FN and *Unknown* classified samples on the synthetic database. (a) CDMs with time to TCA smaller than  $T_1$ , (b) CDMs with time to TCA greater than  $T_1$ . In red letters, it is specified what each in is for each case. Threshold values:  $PoC_0 = 10^{-4}$ ,  $T_1 = 2$  days,  $T_2 = 5$  days,  $Pl_0 = 0$ ,  $A_{Pl,Bel}^* = 0$ . The FEs were built by creating 3 intervals per variable (243 FEs in total).

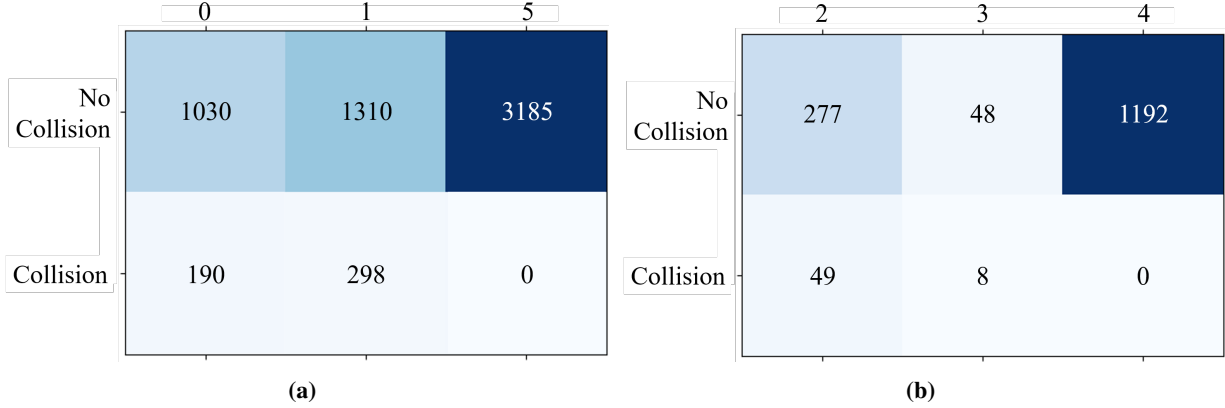


**Fig. 6** Number of TP, TN, FP, FN and *Unknown* classified samples on the synthetic database. (a) CDMs with time to TCA smaller than  $T_1$ , (b) CDMs with time to TCA greater than  $T_1$ . Threshold values:  $PoC_0 = 10^{-4}$ ,  $T_1 = 2$  days,  $T_2 = 5$  days,  $Pl_0 = 1/234$ ,  $A_{Pl,Bel}^* = 0.2$ . The FEs were built by performing 2  $\alpha$ -cuts per variable.

the CDMs high and low probability cases are clearly distinguishable and can be confidently classified as Class 1 (or 2) or Class 0 (or 3).

## B. Comparison Against SDO and CNES

The results in this section show a comparison between the CARA performed with the proposed evidence-based method and the decisions made by real operators in a selected number of real cases. The two operators considered in this study are the ESA's SDO and CNES. Each of them has a different approach to conjunction analysis.

### 1. Space Debris Office Conjunction Risk Assessment

The approach followed by the ESA's SDO is probability-based, relying mainly on the value of the PoC computed with the information from the CDMs, if not the PoC include on the CDM. The following quote may summarise the generic SDO's conjunction risk assessment process: "For a given close approach the last obtained CDM, including the computed risk, can be assumed to be the best knowledge we have about the potential collision and the state of the two objects in question. In most cases, the Space Debris Office will alarm control teams and start thinking about a potential avoidance manoeuvre 2 days prior to the close approach in order to avoid the risk of collision, to then make a final decision 1 day prior"[27]. Nevertheless, each mission monitored by the SDO will have a specific procedure based on this general approach according to its characteristics and constraints.

Under this generic approach, each mission will introduce its own operational constraints (i.e. the time needed to prepare and execute the manoeuvre) and will have its own risk and time threshold. While the time threshold will be highly related to the mission constraints, generally 2 or 3 days to the encounter, the mission team is informed about the possible collision, with a final decision usually made (when possible), 1 day to the conjunction[27]. The risk threshold is determined statistically based on the overall collision risk and the annual frequency of close approaches, trading off the ignored risk and the avoided risk by selecting the risk threshold at the cost of an expected number of annual manoeuvres[1]. Generally, for missions in the LEO regime, a threshold of  $PoC_0 = 10^{-4}$  leads to a risk reduction of around 90% at the expense of 1 to 3 manoeuvres per year. However, a lower threshold, around  $10^{-5}$ , may be selected to ensure potential escalating events are with sufficient time to prepare an avoidance strategy[1].

Thus, when the last CDM's PoC is bigger than the threshold, the event is escalated for further and more detailed analysis. If the risk is still above the threshold at the decision time, a CAM is designed in cooperation with the mission team, whose final decision will be made based on the value of PoC included in the last CDM received before go/no-go decision time. More detailed information on the SDO's CARA process can be found in [1].

In the following, a number of real conjunction events, representative of the different evidence-based criterion classes, are presented. A comparison of the different operational approaches is made. For the next three examples, a simplified scenario only with CDMs generated from the MiniCat database has been considered.

For the next examples, the non-epistemic threshold is given by the mission and the epistemic value has been selected equal to the previous case. Thus, the values for the threshold for the next three examples are those in Table 2.

#### Event #1

This event represents a high-risk scenario provided by the ESA's SDO. The uncertain geometry in the impact plane, with the whole sequence of CDMs and the PoC evolution appear in Fig. 7. Events with PoC above the threshold for times to the TCA greater than  $T_1$  make the event escalate, that is, they are further analysed and possible alerts to the



mission's team can be triggered, while high-risk CDMs received in the last 72 hours start a CAM procedure.

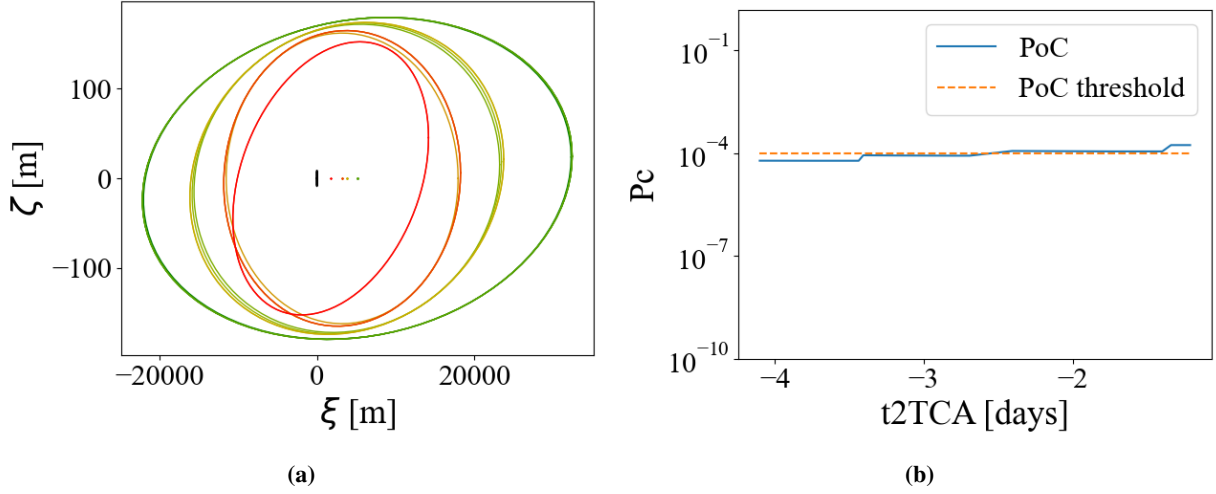


**Fig. 7** CDM information for example in Scenario #1: High-risk event. (a) Uncertain ellipses in the sequence of CDMs. Green ellipses correspond to earlier CDMs, and red ellipses to later CDMs. (b) Evolution of the PoC in the CDMs with the time to the TCA. Blue solid line: PoC; orange dashed line: PoC threshold.

From Fig. 7b, it can be seen that the PoC remains high along the sequence. Even if at the beginning it is below the threshold, its proximity to  $PoC_0$  along with the increasing trend made the operator escalate the event. Finally, the PoC threshold was violated within the last days before the encounter, which led to a CAM execution to reduce the risk of the event.

The robust conjunction analysis has been made following the method presented in Section III. To obtain the DKW bands, a confidence interval parameter of  $\delta = 0.5$  has been selected. The CDMs have been weighed according to the exponential law in Eq. (9). Fig. 8 shows the fitting law after having received all the CDMs (red) along with the value of the combined covariance matrix determinant for the sequence (black). For the fitting law in Fig. 8b, the value of the dimensionless parameters in Eq. (9a) after having received the whole sequence are:  $A = 1.0752, B = 0.9811, C = 0.001716$ . Note that the value of the parameters varies with the number of CDMs received to better fit the covariance determinant evolution up to that time.

The robust analysis was performed for a different number of  $\alpha$ -cuts per uncertain variable:  $\#\alpha\text{-cuts} = \{1, 2, 3, 4, 5, 7\}$ . These cuts led to a number of intervals per variable equal to  $\#\text{intervals} = \{2, 3, 4, 5, 6, 8\}$ , which translates into a number of FEs  $\#\text{FE} = \{32, 243, 1024, 3125, 7776, 16807\}$ , respectively. The  $Pl$  and  $Bel$  curves for the PoC, for each number of cuts, is presented in Fig. 9, after having received the whole sequence of CDMs.

Fig. 9 shows that, although the increasing number of  $\alpha$ -cuts provides a more refined set of curves, their shape and values differ slightly from each other. In this case, the  $Bel$  and  $Pl$  curves overlap for most values of PoC except for a small interval around the  $PoC_0$ , as it could be expected both, from the uncertainty geometry in Fig. 7a and the values of

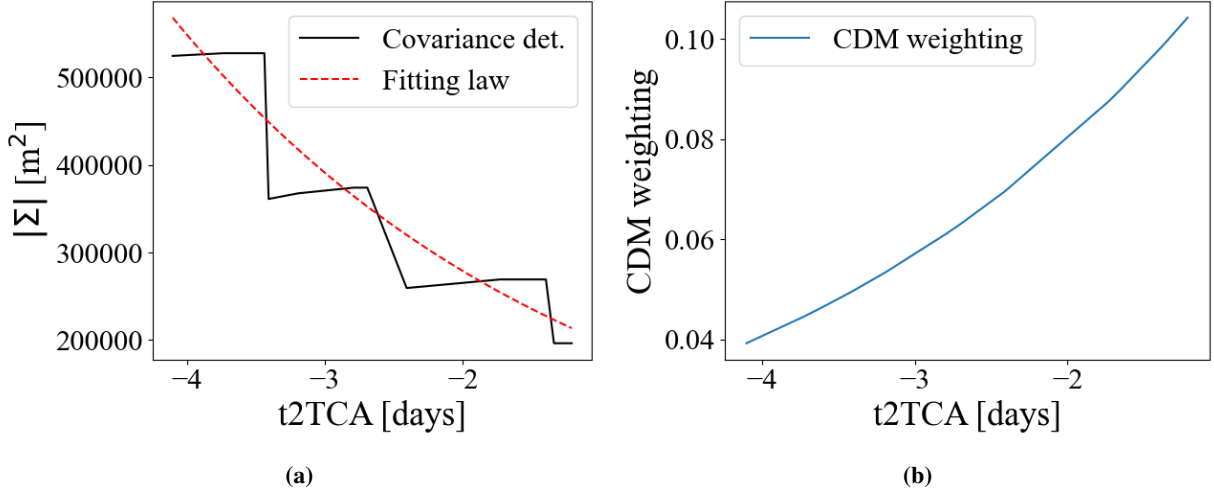


**Fig. 8** Fitting law to weight the CDMs after having received the whole sequence in Scenario #1: High-risk event. (a) Solid black line: value of the determinant from the CDMs, dashed red line: fitting law of the covariance matrix determinant. (b) Weight of the CDMs as a function of the time to the TCA.

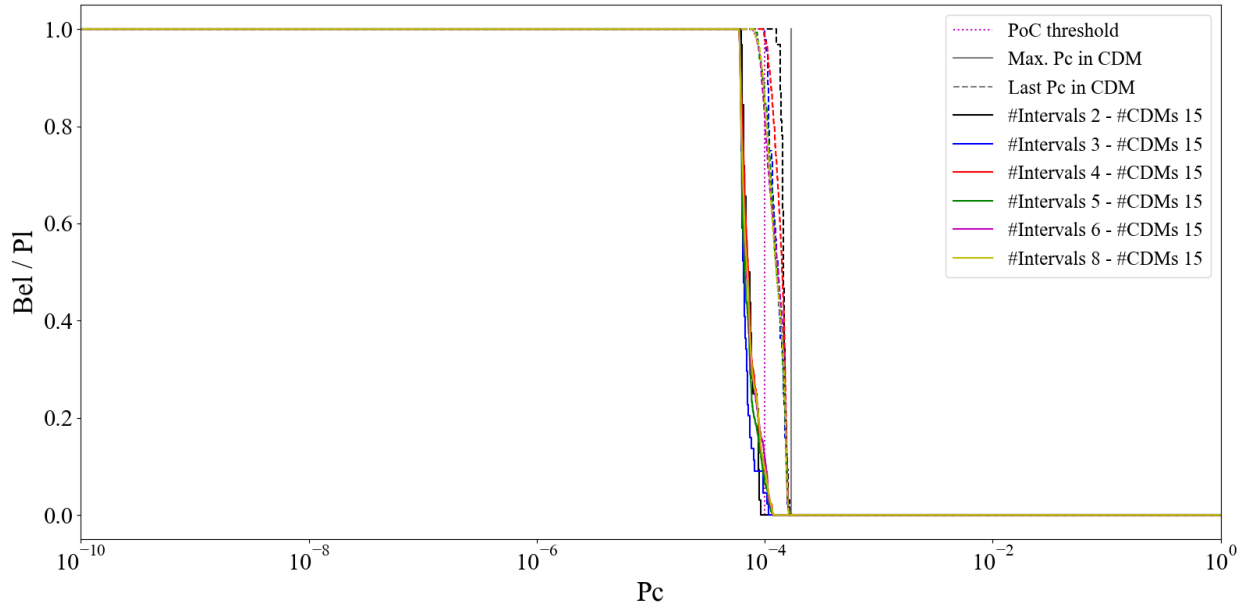


**Fig. 9**  $Pl$  and  $Bel$  of the PoC after having received the whole sequence of CDMs Scenario #1: High-risk event. Solid vertical grey line: maximum PoC in the sequence, dashed vertical grey line: PoC of last CDM, pointed purple line: PoC threshold. For the rest of the colours: Belief in solid lines and Plausibility in dashed lines. Black: 1  $\alpha$ -cut per variable (2 intervals per variable, 32 FEs), blue: 2  $\alpha$ -cuts, red: 3  $\alpha$ -cuts, green: 4  $\alpha$ -cuts, purple: 5  $\alpha$ -cuts, yellow: 7  $\alpha$ -cuts.

the PoC in Fig. 7b. Since the information in the CDM is coherent across the whole sequence, the gap between  $Pl$  and  $Bel$  curves is small, indicating a small epistemic uncertainty affecting this sequence.

Fig. 10 shows the classification, purple solid line, as a function of the time to the TCA from the last received CDM. The figure shows also the PoC directly computed from the CDM.

Initially, the event is classified as Class 4 and rapidly falls to Class 5, since there is little evidence supporting a higher PoC. However, at 2.5 days from TCA the PoC consistently grows above the threshold. Given the little uncertainty in the sequence of CDMs the event is reclassified as Class 1 and a CAM is recommended.

This is the same decision finally taken by the SDO. As seen in Fig. 9, the support for a high value of PoC is high and the gap between the curves (level of uncertainty) is very small. Thus, the outcome for the operator for any decision made in the last days prior to the encounter would be that a manoeuvre should be implemented to reduce the risk of a collision.

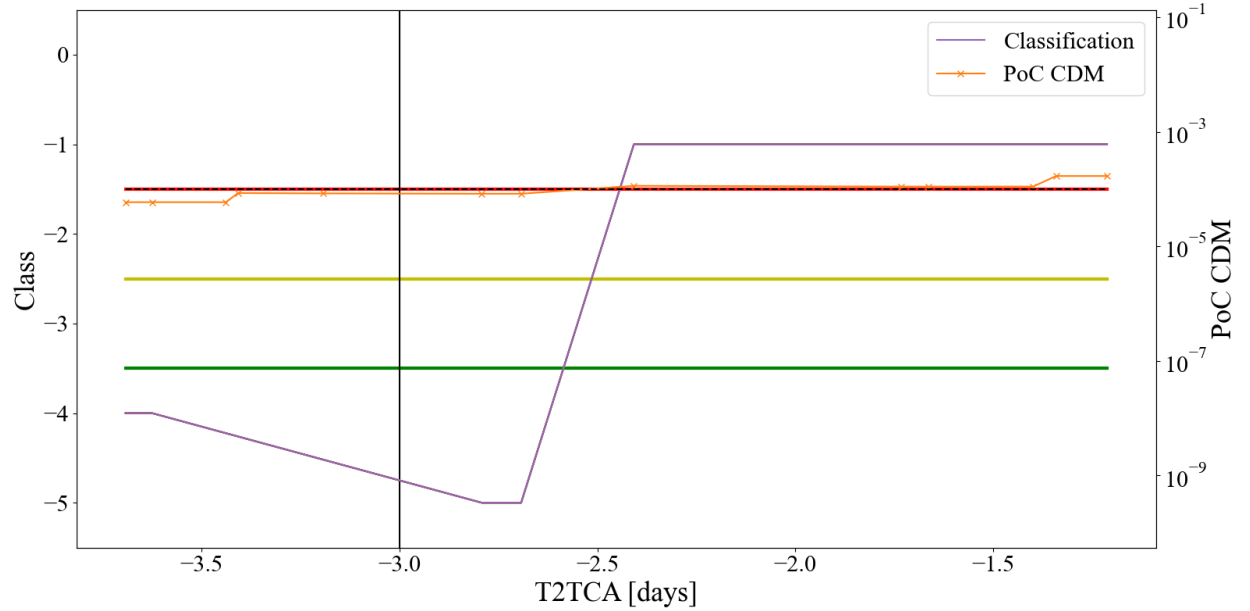


**Fig. 10** Collision risk assessment for Scenario #1: High-risk event. Solid narrow lines: evidence-based classification with different number of  $\alpha$ -cuts:  $\#\alpha\text{-cuts} = \{1, 2, 3, 4, 5, 7\}$  (note that they overlap each other, so only  $\#\alpha\text{-cuts} = 7$  is visible in solid purple). Crossed-solid line: PoC in the CDMs used by SDO for assessment. Horizontal thick lines: evidence approach safety bands: green, low risk-uncertain boundary; yellow, uncertain-high risk boundary; red, mid term high risk-long term high risk boundary. Dashed black line: Risk threshold (overlapping evidence-based high-risk boundary). Vertical black line: decision time threshold.

## Event #2

A similar analysis was done for the Low-risk conjunction event illustrated in Fig. 11, also provided by the ESA's SDO. Opposite to the previous event, in this case, the PoC remains well below the threshold, so no alert is required to be triggered and no CAM is required to be designed or executed.

The robust analysis was performed using the same parameters as before:  $\delta = 0.5$  for the DKW bands, with a different number of  $\alpha$ -cuts:  $\#\alpha\text{-cuts} = \{1, 2, 3, 4, 5, 7\}$  per variable. The CDMs after having received the whole sequence were weighted with the exponential fitting law Eq. (9a) using the following parameters:  $A = 0.6049$ ,  $B = 5.0896$ ,  $C = 0.4518$ .

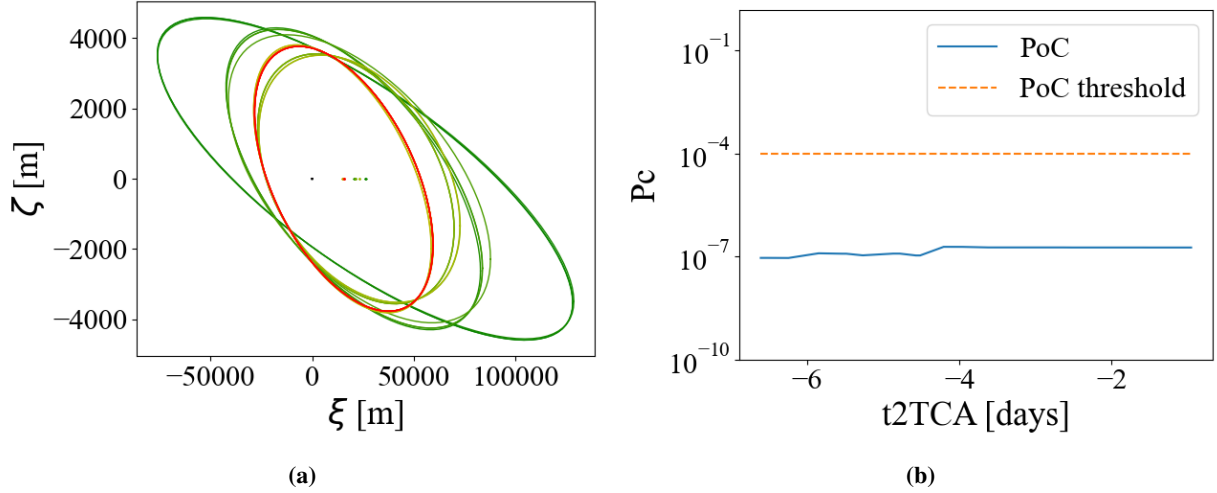


**Fig. 11** CDM information for example in Scenario #2: Low-risk event. (a) Uncertain ellipses in the sequence of CDMs. Green ellipses correspond to earlier CDMs, and red ellipses to later CDMs. (b) Evolution of the PoC in the CDMs with the time to the TCA. Blue solid line: PoC; orange dashed line: PoC threshold.

The fitting law (red) and the combined covariance matrix determinant in the CDMs (black) appear in Fig. 12. Note the convergence in the second half of the sequence.

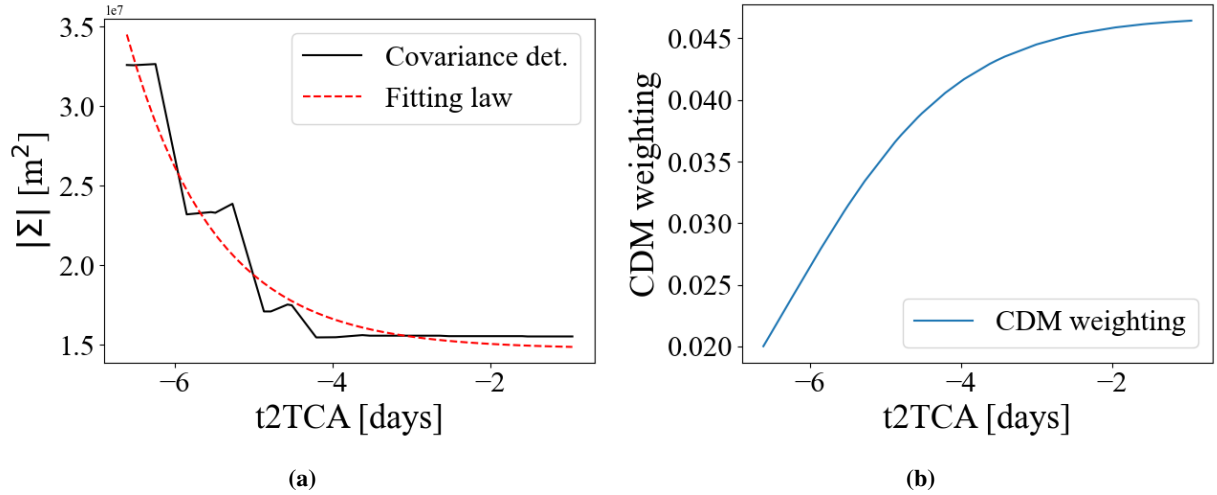


**Fig. 12** Fitting law to weight the CDMs after having received the whole sequence in Scenario #2: Low-risk event. (a) Solid black line: value of the determinant from the CDMs, dashed red line: fitting law of the covariance matrix determinant. (b) Weight of the CDMs as a function of the time to the TCA.

In Fig. 13, the corresponding  $Pl$  and  $Bel$  curves on the value of PoC after having received all the CDMs of the event are shown. Again, increasing the number of  $\alpha$ -cuts makes the curves smoother and shows a converging trend, but does not change the overall confidence in the value PoC. The maximum value of PoC with some supporting evidence is well below the threshold, indicating that the event can be deemed to be safe. However, the left-most part of the  $Bel$  and  $Pl$  curves shows a significant gap. This can be explained by the fact that the ellipses are not too different from each

other (Fig. 11a) and they tend to converge to a single ellipse for the later CDMs, as shown in Fig. 11b. Thus, the initial information content in each CDM tends to support lower values of PoC, which explains the lower value of  $Bel$  on the left of the graph. However, due to the concentration of information around the later CDMs, the big drop both in  $Pl$  and  $Bel$  occurs at  $PoC \sim 10^{-7}$ .

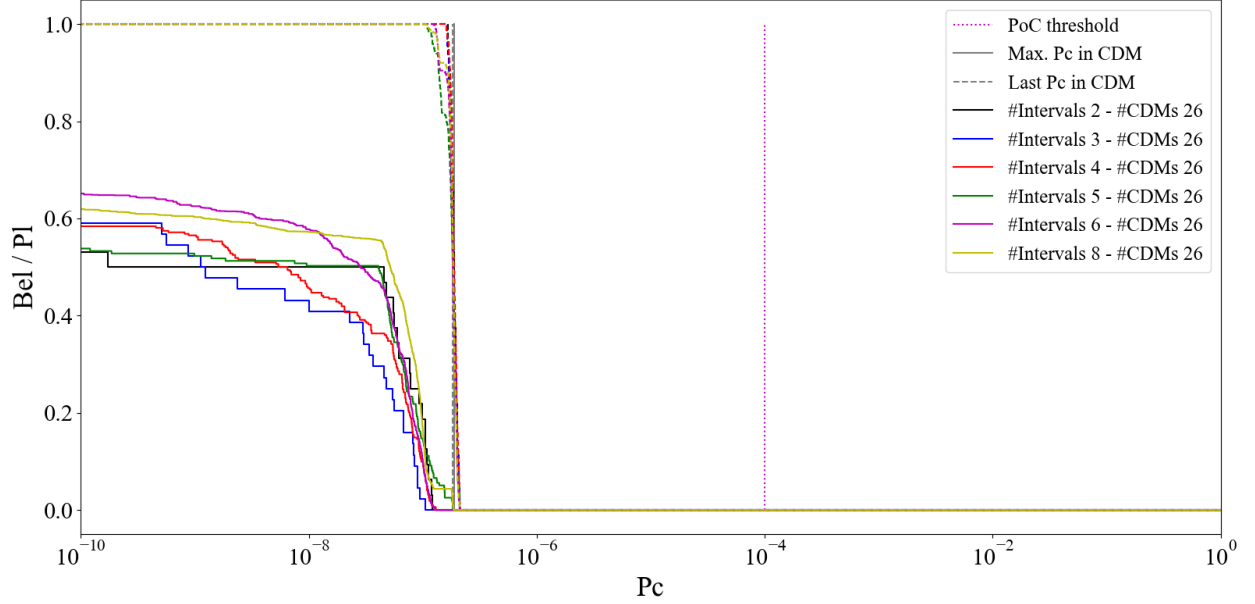


**Fig. 13**  $Pl$  and  $Bel$  of the PoC after having received the whole sequence of CDMs Scenario #2: Low-risk event. Solid vertical grey line: maximum PoC in the sequence, dashed vertical grey line: PoC of last CDM, pointed purple line: PoC threshold. For the rest of the colours: Belief in solid lines and Plausibility in dashed lines. Black: 1  $\alpha$ -cut per variable (2 intervals per variable, 32 FEs), blue: 2  $\alpha$ -cuts, red: 3  $\alpha$ -cuts, green: 4  $\alpha$ -cuts, purple: 5  $\alpha$ -cuts, yellow: 7  $\alpha$ -cuts.

Finally, the conjunction assessment for the whole sequence is shown in Fig. 14. Despite the greater uncertainty with respect to the previous scenario, it affects only very small values of the PoC. For values of the PoC greater than  $10^{-7}$ , there is no uncertainty: those higher values do not receive any support ( $Pl = Bel = 0$ ), meaning higher values of PoC are not likely to happen according to the available evidence. Thus, the event is initially classified as Class 4 ( $t2TCA > T_1$ ) and then dropped to Class 5 ( $t2TCA \leq T_1$ ) for the whole sequence, meaning that no further action should be taken by the operator. This is the same decision made by the SDO.

### Event #3

This last event is affected by a significant level of uncertainty. The encounter geometry and the evolution of the PoC in the CDMs are shown in Fig. 15. Despite the initial higher risk, with values of PoC close to the threshold, the final decision of the SDO was not to take any further action. This decision is driven by the latest values of PoC, notably lower than the initial ones, and considerably below  $PoC_0$ .

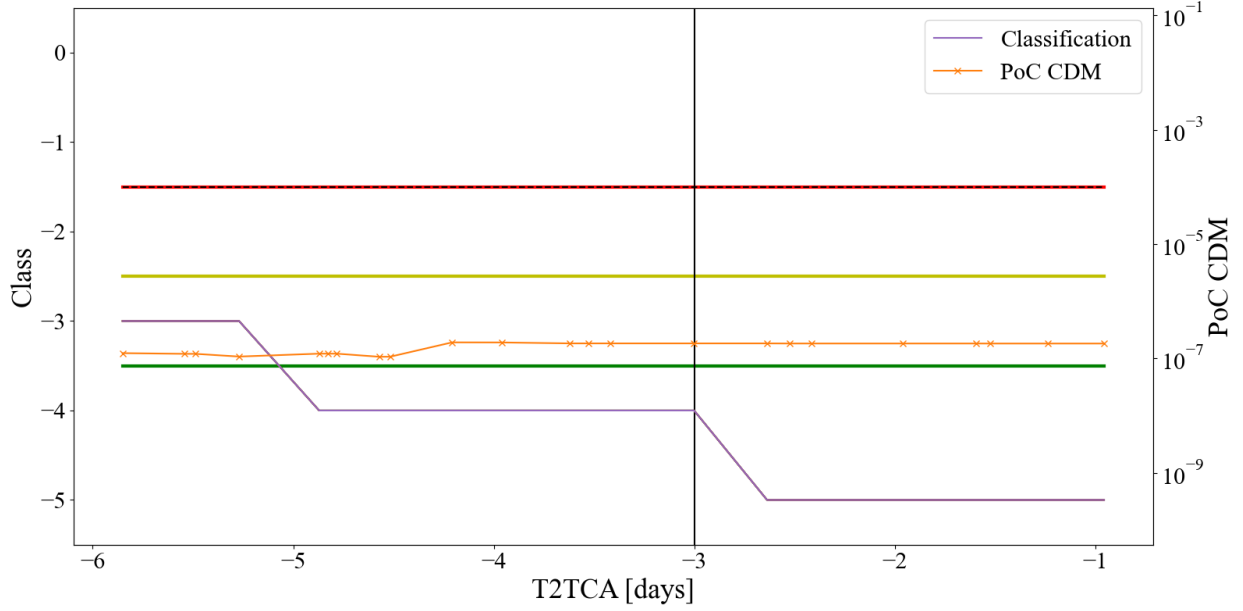


**Fig. 14** Collision risk assessment for Scenario #2: Low-risk event. Solid narrow lines: evidence-based classification with different number of  $\alpha$ -cuts:  $\#\alpha\text{-cuts} = \{1, 2, 3, 4, 5, 7\}$  (note that they overlap each other, so only  $\#\alpha\text{-cuts} = 7$  is visible in solid purple). Crossed-solid line: PoC in the CDMs used by SDO for assessment. Horizontal thick lines: evidence approach safety bands: green, low risk-uncertain boundary; yellow, uncertain-high risk boundary; red, mid term high risk-long term high risk boundary. Dashed black line: Risk threshold (overlapping evidence-based high-risk boundary). Vertical black line: decision time threshold.

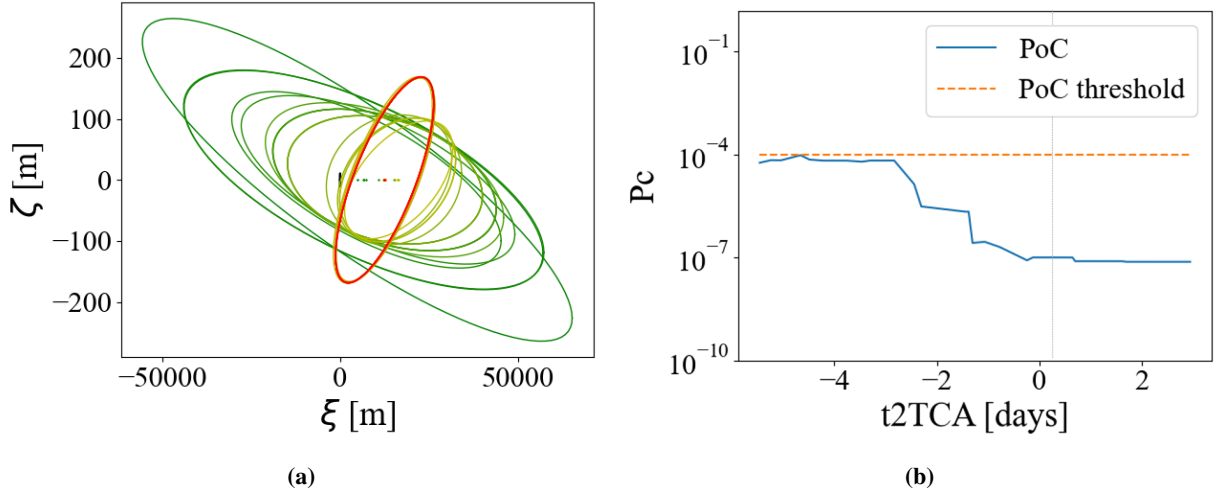


**Fig. 15** CDM information for example in Scenario #3: Uncertain event. (a) Uncertain ellipses in the sequence of CDMs. Green ellipses correspond to earlier CDMs, and red ellipses to later CDMs. (b) Evolution of the PoC in the CDMs with the time to the TCA. Blue solid line: PoC; orange dashed line: PoC threshold, vertical dashed grey line: TCA.

The robust analysis was performed with the same parameters as before:  $\delta = 0.5$  for the DKW bands. The exponential fitting law Eq. (9a) to weight the CDMs, after having received the whole sequence, uses the following parameters  $A = 0.7917$ ,  $B = 7.1471$ ,  $C = 0.1858$  and is shown in Fig. 16 (red) along with the covariance matrix determinant from

the CDMs (black).

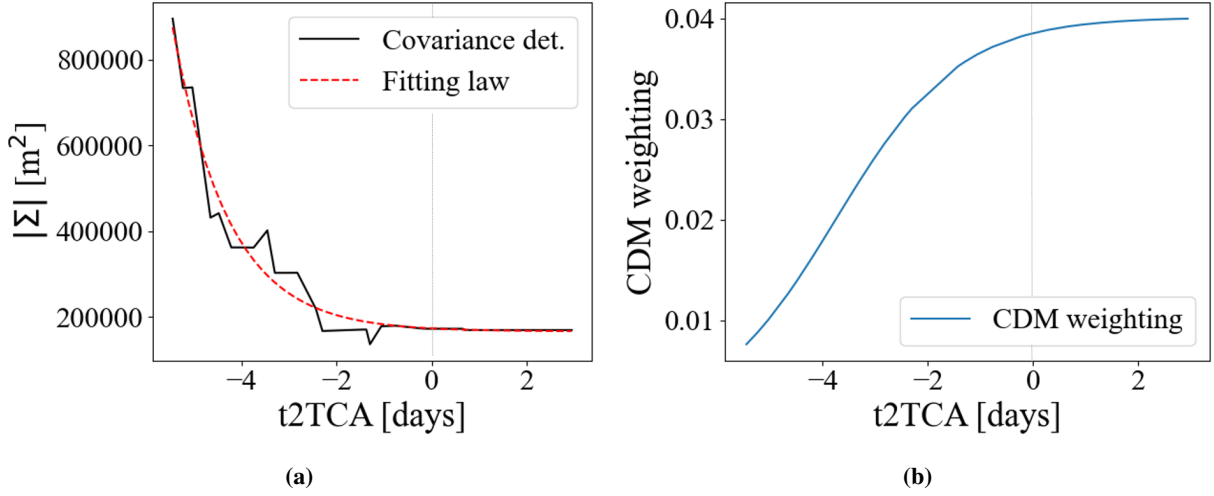


**Fig. 16** Fitting law to weight the CDMs after having received the whole sequence in Scenario #3: Uncertain event. (a) Solid black line: value of the determinant from the CDMs, dashed red line: fitting law of the covariance matrix determinant. Vertical dashed grey line: TCA. (b) Weight of the CDMs as a function of the time to the TCA. Vertical dashed grey line: TCA.

The  $Pl$  and  $Bel$  curves for the PoC were for different  $\alpha$ -cuts:  $\#\alpha\text{-cuts} = \{1, 2, 3, 4, 5, 7\}$ . The curves are shown in Fig. 17. In this case, there is a significant gap between  $Pl$  and  $Bel$  for all the values of PoC for which  $Pl > 0$ . This uncertainty (or level of disagreement between CDMs) can be seen in Fig. 15a, showing the rotation experienced by the uncertainty ellipses from the beginning of the sequence to the latest CDMs. This level of uncertainty also made that, despite the latest CDMs (which have a bigger relative weight associated) containing lower values PoC, from the robust analysis, higher values of PoC receive enough support. As in the previous scenario, the ellipses tend to converge in the second half of the sequence, however, the difference with respect to the first one is much bigger, so this convergence does not compensate for the discrepancy as before.

The level of uncertainty is also reflected in the classification of the event (Fig. 18). Firstly, there is a slight influence of the number of  $\alpha$ -cuts for some values of  $t2TCA$ , although, for most of the  $t2TCA$  instances, there is a common outcome for most of the cases. Secondly and most importantly, the influence of the uncertainty in the sequence of CDMs appears in the outcome of the event: Class 3 ( $t2TCA > T_1$ ) and Class 0 ( $t2TCA \leq T_1$ ), which are the classes encoding the uncertain events. Also, in this case, unlike the previous ones, a discrepancy between the SDO action (not to take any further action) with the final outcome of the evidence-based classification. The evidence-based system suggests performing a CAM due to the possibility of high risk ( $Pl(PoC_0) > Pl_0$ ) associated with the uncertainty ( $A > A_{Pl,Bel}$ ) and proximity of the event ( $t2TCA < T_1$ ). On the contrary, the SDO action was to dismiss the conjunction due to the reduction in the risk on the later CDMs (decrease on the solid-crossed orange line).

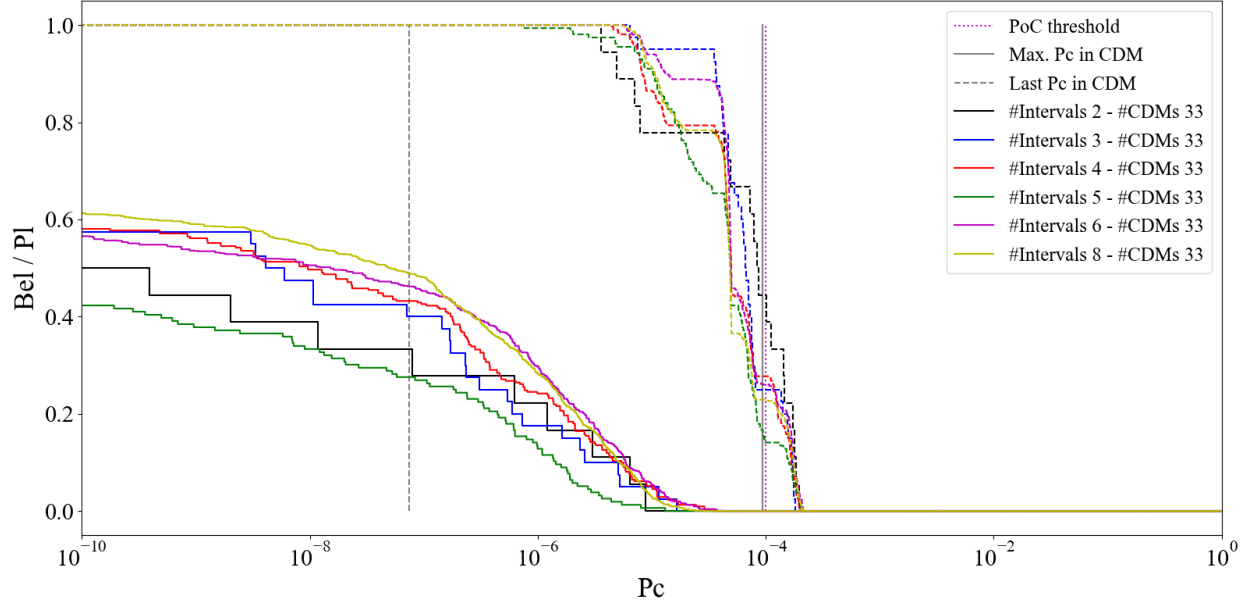


**Fig. 17** *Pl* and *Bel* of the PoC after having received the whole sequence of CDMs Scenario #3: Uncertain event. Solid vertical grey line: maximum PoC in the sequence, dashed vertical grey line: PoC of last CDM, pointed purple line: PoC threshold. For the rest of the colours: Belief in solid lines and Plausibility in dashed lines. Black: 1  $\alpha$ -cut per variable (2 intervals per variable, 32 FEs), blue: 2  $\alpha$ -cuts, red: 3  $\alpha$ -cuts, green: 4  $\alpha$ -cuts, purple: 5  $\alpha$ -cuts, yellow: 7  $\alpha$ -cuts.

## 2. CNES Conjunction Risk Assessment

As shown in Eq. (1), the value of the PoC is very sensitive to the position covariance matrix of the objects involved in the encounter, whose value from CDM can be underestimated or overestimated. In order to have a value that accounts for this miss-estimation on the CDMs covariance matrices, CNES operators use Java for Assessment of Conjunctions (JAC) for conjunction risk assessment[10, 11]. JAC employs the so-called scaled Probability of Collision (sPoC), instead of the PoC, as the metric to make decisions[31]. To compensate for the possible lack of realism of the covariance matrices, the scaling factor  $k_p \in K_P$  and  $k_s \in K_S$  are employed to scale up and down. The sPoC is obtained by solving Eq. (12) as the maximum value of the PoC among the different combinations of scaling factors for the primary and secondary objects.

$$\begin{cases} sPoC = \max_{K_P, K_S} (PoC) \\ \text{with } \Sigma = k_p^2 \Sigma_p + k_s^2 \Sigma_s \end{cases}, \quad (12)$$

where  $\Sigma_p$  and  $\Sigma_s$  are, respectively, the primary and secondary covariance matrices in the last CDM associated with the conjunction event.

The default bounds of  $K_P$  and  $K_S$  in JAC software are  $[0.25, 4]$ , although more realistic boundaries can be obtained based on the sequence of CDMs. However, it goes at the expense of making two assumptions: the sequence of CDMs represents a set of samples from an underlying distribution, and the last CDM is given more relevance. Thus, using the



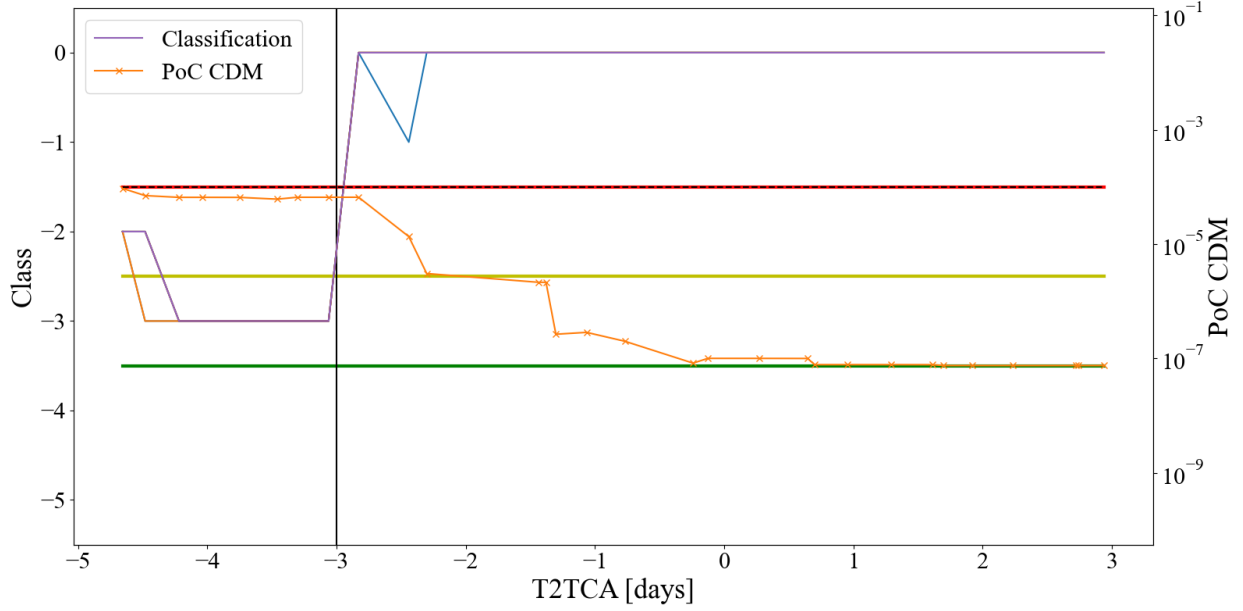


**Fig. 18** Collision risk assessment for Scenario #3: Uncertain event. Solid narrow lines: evidence-based classification with different number of  $\alpha$ -cuts:  $\#\alpha$ -cuts =  $\{1, 2, 3, 4, 5, 7\}$  (note that they overlap each other, so only  $\#\alpha$ -cuts = 7 is visible for all  $t2TCA$  in solid purple;  $\#\alpha$ -cuts = 1 in solid blue and  $\#\alpha$ -cuts = 2 in solid orange are visible at one  $t2TCA$  each). Crossed-solid line: PoC in the CDMs used by SDO for assessment. Horizontal thick lines: evidence approach safety bands: green, low risk-uncertain boundary; yellow, uncertain-high risk boundary; red, mid term high risk-long term high risk boundary. Dashed black line: Risk threshold (overlapping evidence-based high-risk boundary). Vertical black line: decision time threshold. Vertical dashed grey line: TCA.

last CDMs as the reference, it is possible to compute the Mahalanobis distance of previous CDMs uncertainty ellipses, and assuming the uncertainty in position follows a Gaussian distribution, the Mahalanobis distance must follow a  $X^2$  distribution with 3 degrees of freedom. Performing a Kolmogorov-Smirnov (KS) test between the actual distribution and the theoretical one, and setting a desired level of realism, it is possible to find more realistic boundaries for  $K_P$  and  $K_S$ . More details can be found in [31].

CNES decision-making is then based on both geometric criteria and sPoC-based criteria. Events with values of  $sPoC > 5 \cdot 10^{-4}$  are treated as High-Interest Event, the more risky classification level (red level). For values of  $10^{-4} < sPoC < 5 \cdot 10^{-4}$ , the event is classified as an Interest Event, the second level of risk (orange level). If the value of the  $sPoC$  is below those thresholds, caution geometric criteria are applied: miss distance below 1 km or radial distance below 200 m. Note that these threshold values are the default ones and may change from mission to mission. If the CDMs are received early in time (generally, around 4-5 days before the encounter), no alerts are raised independently of the level of risk of the conjunction, although the event is decided to be under study if some of the criteria are violated. For later CDMs, alerts may be raised according to the level of risk of the event (orange or red). Finally, if the high risk continues after the decision time (usually 2 days before the encounter), a final decision is made before the TCA.

In the following, a real close encounter faced by CNES and the comparison between operational approach is shown.

#### Event #4: CNES approach

This scenario presents a high-risk collision case for a real close encounter where CNES had to implement a manoeuvre to reduce the risk. This scenario is interesting since it allows comparing the CNES approach, based on the sPoC with both the robust approach proposed in this paper and the approach based exclusively on the value of the PoC.

Fig. 19a shows the geometry of the event, where initial CDMs (greener colours) suggested a lower PoC, while later CDMs approach to the HBR. This is reflected in the value of the PoC in Fig. 19b, where the value of the PoC increases when approximating to the encounter. These figures also show the sPoC which already suggests from the beginning a higher risk than the value of the CDM. It can be seen how the sPoC already predicted a value of risk above  $10^{-4}$ , close to the value of PoC for the last CDM, while the PoC in the sequence of CDMs required to be much closer to the encounter to proposed such values, and even then, with a less stable behaviour. This is reflected in the decision-making process followed by CNES's operators on this event: the event is catalogued as *High-Interest Event*, meaning careful monitoring should be taken, from the 12<sup>th</sup> CDM (2.96 days before the TCA), and a final decision for performing a manoeuvre is taken 30 hours before the encounter. Note that the last CDM received by the decisions time indicates a  $PoC < 10^{-5}$ , well below the risk threshold, while the sPoC indicates a risk above  $10^{-3}$ , which aligns better with the last three CDMs received between the decision time and the CAM execution time).

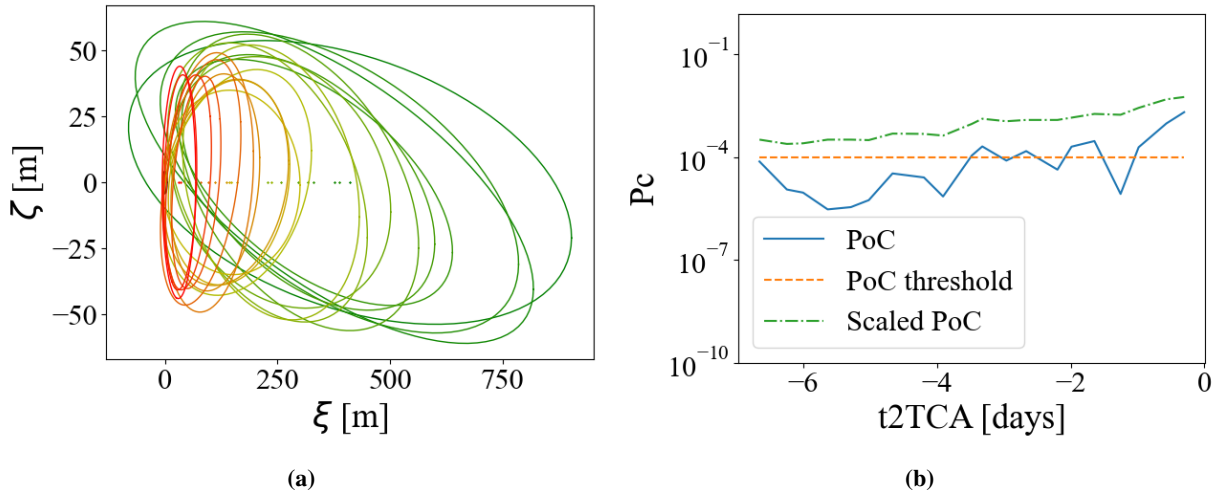


**Fig. 19** CDM information for example in Scenario #4. (a) Uncertain ellipses in the sequence of CDMs. Green ellipses correspond to earlier CDMs, and red ellipses to later CDMs. (b) Evolution of the PoC in the CDMs with the time to the TCA. Blue solid line: PoC; dashed-dotted line: sPoC; orange dashed line: PoC threshold.

The evidence-based analysis was performed following the same approach as for the SDO cases and with the same thresholds (Table 2), with  $\#intervals = \{2, 3, 4, 5, 6, 8\}$  intervals per variable and CDM weighed according to the exponential law in Fig. 20.

The  $Pl$  and  $Bel$  corresponding to the analysis after having received the whole sequence of CDM is shown in Fig. 21,

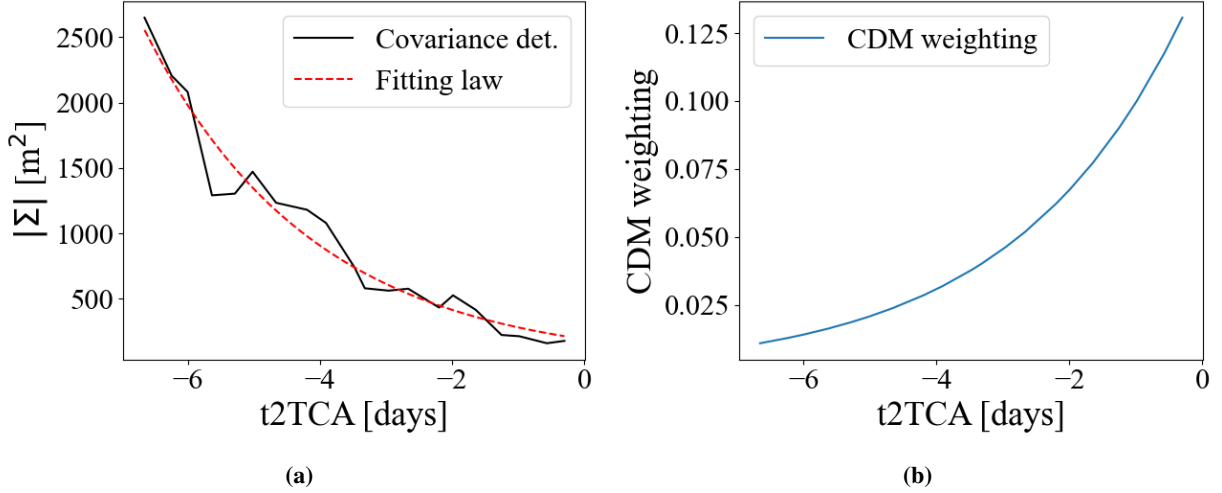


**Fig. 20** Fitting law to weight the CDMs after having received the whole sequence in Scenario #4. (a) Solid black line: value of the determinant from the CDMs, dashed red line: fitting law of the covariance matrix determinant. (b) Weight of the CDMs as a function of the time to the TCA.

and the classification sequence for the event for different numbers of intervals is shown in Fig. 22. It can be seen from the  $Pl$  and  $Bel$  curves figures, that the high risk is considered plausible: the value of  $Pl(PoC_0)$  is equal or very close to 1, and  $Pl(sPoC) > 0$  along the whole time series:  $Pl = 0$  at  $PoC \sim 10^{-2}$ , while  $\max(sPoC) = 5 \cdot 10^{-3}$ . However, the gap between curves is very high, indicating a degree of uncertainty in the sequence of CDMs. This is due to the initial CDMs being very different from the last ones and the PoC oscillating below and above the threshold. This led to a classification of the event as Class 0. A CAM is proposed to the operator, and it is suggested, already, very soon in the time series. However, the avoidance strategy is proposed, mainly, due to the uncertainty of the event.

Although this event is classified in the same fashion as Event 3, the supporting evidence is quite different. Event 4 has a  $Pl \approx 1$  and  $Bel$  different from zero at  $PoC_0$  while Event 3 as  $Bel = 0$  and  $Pl < 0.2$  at  $PoC_0$ . This means that although in this paper we opted for a very conservative classification of the events such that both Events 3 and 4 fall in the same uncertainty class, a simple analysis of the  $Bel$  and  $Pl$  curves would suggest that the available evidence for Event 4 supports a high probability of collision, up to  $10^{-2}$  in fact, while for Event 3 the supporting evidence at  $PoC_0$  is quite low.

### C. Statistical Analysis of CAM Executions

After having compared the proposed evidence-based conjunction assessment approach against real operations on specific cases, in this section we compare how many CAMs are executed or recommended in a large number of real conjunctions.

The selected mission is the ESA's SWARM-A satellite, orbiting in the LEO regime (circular polar orbit of 87.7 deg at 511 km of altitude), dedicated to studying the Earth's magnetic field as part of a constellation of three satellites.

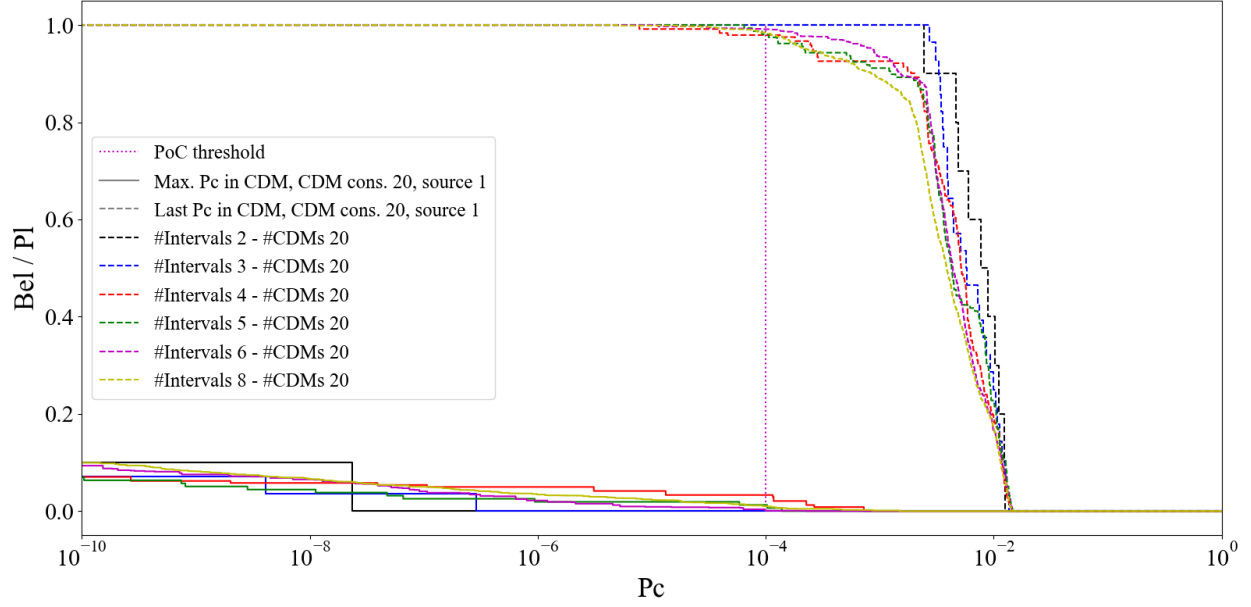


**Fig. 21**  $Pl$  and  $Bel$  of the PoC after having received the whole sequence of CDMs Scenario #4. Solid vertical grey line: maximum PoC in the sequence, dashed vertical grey line: PoC of last CDM, pointed purple line: PoC threshold. For the rest of the colours: Belief in solid lines and Plausibility in dashed lines. Black: 1  $\alpha$ -cut per variable (2 intervals per variable, 32 FEs), blue: 2  $\alpha$ -cuts, red: 3  $\alpha$ -cuts, green: 4  $\alpha$ -cuts, purple: 5  $\alpha$ -cuts, yellow: 7  $\alpha$ -cuts.

The mission thresholds to trigger conjunction alerts are  $PoC_0 = 10^{-4}$  and  $T_1 = 72$  hours. Thus, any satellite with a PoC above the threshold in the last 3 days would escalate and would require further analysis, and eventually, a possible CAM design or execution. Nevertheless, encounters presenting a higher risk or an increasing trend before  $T_1$  may be escalated if the operator considers that there is a potential risk for the mission. Finally, the go/no-go decision is subject to operational constraints: the time required to design a CAM after receiving the triggering manoeuvre, the possibility to upload and check the design manoeuvre and the ground station availability.

The database of CDMs includes alerts from 2015 to 2022, with a total of 36,072 events. Overall, most of the events in the database did not represent a threat to the satellite, with only 20 representing escalated events. As explained before, an escalated event is an encounter where the PoC, or the PoC trend, suggests that the conjunction may be high risk. From those escalated events, only 2 required a CAM to be executed.

The evidence-based analysis was performed with the same thresholds as the previous study cases (Table 2):  $PoC_0 = 10^{-4}$ ,  $T_1 = 3$  days,  $T_2 = 5$  days,  $Pl_0 = 1/243$ ,  $A_{Pl,Bel}^* = 0.2$ , with  $\underline{PoC} = 10^{-30}$ , and  $A_{Pl,Bel} = 3$ . The DKW bands were obtained assuming a confidence interval of  $\delta = 0.5$ . As shown before, a higher number of  $\alpha$ -cuts would refine the  $Pl$  and  $Bel$  curves, providing closer curves that better represent the actual epistemic uncertainty. However, this is at the expense of increasing the computational cost and with limited impact on the final classification. Thus 2  $\alpha$ -cuts (3 intervals) per variable, with a total of 243 FEs per analysis were used.

Since the robust analysis lacks the real information available in the actual operation of the satellite that may have

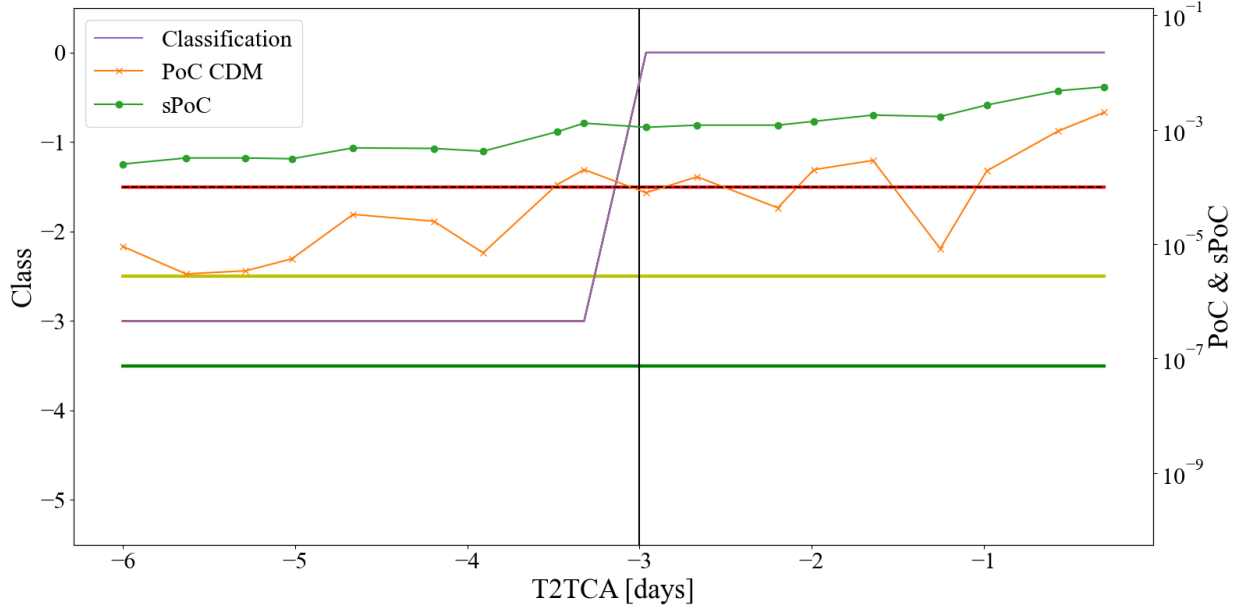


**Fig. 22** Collision risk assessment for Scenario #4. Solid narrow lines: evidence-based classification with different number of  $\alpha$ -cuts:  $\#\alpha$ -cuts =  $\{1, 2, 3, 4, 5, 7\}$  (note that they overlap each other, so only  $\#\alpha$ -cuts = 7 is visible in solid purple). Crossed-solid line: PoC in the CDMs used by SDO for assessment. Horizontal thick lines: evidence approach safety bands: green, low risk-uncertain boundary; yellow, uncertain-high risk boundary; red, mid-term high risk-long term high risk boundary. Dashed black line: Risk threshold (overlapping evidence-based high-risk boundary). Vertical black line: decision time threshold.

affected the operator decision (for example, the ground station availability or the mission constraints), the statistics were computed at four decision times:  $T_d = 3$  days to the TCA, corresponding with the mission time threshold,  $T_1$ ;  $T_d = 2$  days to the TCA, allowing for more data to arrive;  $T_d = 1$  day to the encounter, the usual go-no go decision time in ESA's missions [1]; and the epoch of the last CDM in the sequence,  $T_d = 0$ , situation assuming there is no operational constraint to make the final decision and all information is, thus, available.

Table 3 includes the results from the analysis, compared with the actual statistics provided by the SDO. It is important to bear in mind the differences between the approaches. An event classified with the evidence-based approach as Class 3 or Class 0 (*Uncertain*) would not correspond, necessarily, with an escalated event, since the meaning is different: while an escalated event assumes a certain level of risk, a Class 0 or 3 suggests a degree of uncertainty that requires further investigation before making a final decision. This further investigation might be simply limited to an inspection of the *Bel* and *Pl* curves as in cases 3 and 4 above or might require additional observations. Note that for Class 1 events the recommendation is to perform a CAM, while a Class 0 indicates the occurrence of an uncertain event close in time, which would recommend a CAM as a conservative action.

From Table 3, some conclusions can be derived. The number of manoeuvres proposed by the evidence-based approach is similar to the number of CAMs proposed by the SDO operators. Even if the  $Pl_0$  threshold is quite low,

**Table 3** Results from the statistical analysis on the SWARM-A mission, with the SDO approach and the evidence-based approach. Threshold:  $PoC_0 = 10^{-4}$ ,  $T_1 = 3$  days,  $T_2 = 5$  days,  $Pl_0 = 1/243$ ,  $A_{Pl,Bel}^* = 0.2$  ( $A_{Pl,Bel} = 3$ ). Partition with 2  $\alpha$ -cuts per variable.

SDO		Evidence-based				
# events		# events	$T_d = 3$	$T_d = 2$	$T_d = 2$	$T_d = 0$
Total	36,072	Total	24,296	27,918	32,108	36,072
Escalated	20	Unc.	120	130	172	293
CAM	2	CAM	1	2	3	2

the number of events escalating to Class 1 remains small. Thus the system is robust enough to remove false negatives but without introducing many false alerts. Also, the number of CAMs remains roughly constant independently of the decision time.

On the other hand, the evidence-based system found many more uncertain cases than the SDO. The number of Class 0 events is between 6 and 15 times higher than the number of escalated events proposed by ESOC. It is here where the evidence-based system differentiates from the probabilistic approach used by ESOC. Those cases are compounded by all the events with enough support to indicate that a collision may occur because  $Pl(PoC_0) > Pl_0$ , but are deemed uncertain because  $A > A_{Pl,Bel}$ . As in the case of Event 3, many of these cases display a low  $Pl$  and zero  $Bel$ . Others present conflicting CDM, that cannot be resolved without further observations, or a high  $Pl$  for high PoC values, as in Event 4 but with a low  $Bel$ .

Note that the percentage of events in this category increases when delaying the decision. This indicates a growing disagreement among CDMs in the sequence as the time approaches TCA, an aspect usually overlooked by probabilistic-based approaches.

## V. Conclusions

This work presented a methodology to quantify and model the epistemic uncertainty in a sequence of CDMs, and exploit this quantification to make robust decisions about conjunction events. The method was tested against real operations on a number of real scenarios. The key working assumption was that the value of the miss distance and covariance matrix in each CDM were drawn from a set of unknown distributions. The DKW inequality was used to build bounds on this set and derive a set of focal elements, with associated probability mass supporting a given value of the probability of collision.

The collection of focal elements was used to compute the  $Pl$  and  $Bel$  on a given value of the PoC. The  $Pl$  at  $PoC_0$ , or  $Pl_0$  was proposed as a further criterion to make a decision on the actual severity of a conjunction event, while the difference between  $Pl$  and  $Bel$ , or  $A_{Pl,Bel}$ , was proposed as a measure of the uncertainty in the quantification of the PoC.

This methodology was first tested on a synthetic database of CDMs and then applied to a number of real scenarios

with real sequences of CDMs. A very conservative value of  $Pl_0$  was proposed to eliminate all possibilities to confuse a collision for a non-collision event.

It was found that when the set of CDMs contains coherent information over the whole time series, the proposed classification system suggests the same decisions normally made by the ESA SDO. When the sequence of CDMs presents a higher degree of variability or a degree of inconsistency the proposed evidence-based approach provides a quantification of the related uncertainty and classifies the events accordingly.

A comparison with CNES approach, based on the concept of sPoC, has shown how the proposed evidence-based approach provides consistent decisions but with a higher level of information on the uncertainty in the decision. By comparing the ESA and CNES uncertain cases, it was also found that a further inspection of the  $Pl$  and  $Bel$  curves offers a way to disambiguate the events as the different evolution of PoC over time is reflected in a lower or higher value of  $Pl$  and  $Bel$ .

Finally, a statistical analysis on a database of real encounters of an ESA mission showed that the number of recommended CAMs is similar but the evidence-based approach tends to detect a higher number of uncertain cases that require further analysis.

Although in our analysis no operational constraints were considered, the number of detected uncertain cases suggests that relying only on the last CDM may be too optimistic while the scaled PoC approach might be too pessimistic without a further uncertainty quantification. In relation to the uncertain cases, different situations can be found which may lead the operator to take different actions. Further analysis on the treatment of these scenarios should be taken and a threshold tuning analysis using virtual datasets or a mixed dataset of real and virtual CDMs may help on this task.

Future work will need to consider the correlation and interdependence among variables during the construction of the focal elements. Furthermore, the current databases of real CDMs do not represent a controlled set of events, because the actual outcome is unknown. A representative synthetic database would greatly help in improving the classification system. Last but not least, machine learning can be used to directly classify events from the time series of CDMs. This approach represents an extension of what was already proposed by the authors and would improve on current efforts to predict the last CDM with machine learning as it would embed a quantification of uncertainty in the prediction.

## **Funding Sources**

This work was funded by the European Space Agency, through the Open Space Innovation Platform (OSIP), "Idea I-2019-01650: Artificial Intelligence for Space Traffic Management".

## **Acknowledgments**

The authors would like to thank CNES-Toulouse and the DOA/SME/SE Office for the opportunity to research with them and for sharing really valuable information with us. More specifically, we would like to thank François Laporte for

the insightful discussions during the approach development. The authors would like to thank the ESA's Space Debris Office at ESOC for providing both very useful data and feedback on this work during the research stays at their facilities.

## References

- [1] Merz, K., Braun, V., Benjamin Bastida, V., Flohrer, T., Funke, Q., Krag, H., and Lemmens, S., "Current collision avoidance service by ESA's Space Debris Office," *7<sup>th</sup> European Conference on Space Debris*, ESA/ESOC, Darmstadt, Germany, 18-21 April 2017.
- [2] Newman, L., Mashiku, A., Hejduk, M., Johnson, M., and Rosa, J., "NASA Conjunction Assessment Risk Analysis (CARA) updated requirements architecture," *AAS/AIAA Astrodynamics Specialist Conference*, Portland, Maine, US, 2019.
- [3] Recommended Standard: CCSDS 508.0-B-1, "Recommendation for space data system standards. Conjunction data message," Tech. rep., CCSDS, Washington, DC, USA, Jun. 2013. <https://public.ccsds.org/Pubs/508x0b1e2s.pdf>.
- [4] Aristoff, J. M., Horwood, J. T., Singh, N., and Poore, A., "Nonlinear uncertainty propagation in orbital elements and transformation to Cartesian space without loss of realism," *AAS/AIAA Astrodynamics Specialist Conference*, San Diego, CA, US, 2014.
- [5] Cano, A., Pastor, A., Escobar, D., Míguez, J., and Sanjurjo-Rivo, M., "Covariance determination for improving uncertainty realism in orbit determination and propagation," *Advances in Space Research. Space Environment Management and Space Sustainability*, Vol. 72, No. 7, 2023, pp. 2759–2777. DOI: <https://doi.org/10.1016/j.asr.2022.08.001>.
- [6] Pinto, F., Acciarini, G., Metz, S., Boufelja, S., Kaczmarek, S., Merz, K., Martínez-Heras, J., Letizia, F., Bridges, C., and Baydin, A., "Towards automated satellite conjunction management with bayesian deep learning," *AI for Earth Sciences Workshop at NeurIPS*, 2020. URL [https://nips.cc/virtual/2020/public/workshop\\_16105.html](https://nips.cc/virtual/2020/public/workshop_16105.html).
- [7] Acciarini, G., Pinto, F., Letizia, F., Martínez-Heras, J., Merz, K., Bridges, C., and Güneş Baydin, A., "Kessler: a machine learning library for spacecraft collision avoidance," *8<sup>th</sup> European Conference on Space Debris*, ESA/ESOC, Darmstadt, Germany, 2021.
- [8] Uriot, T., Izzo, D., Simões, L., Abay, R., Einecke, N., Rebhan, S., Martinez-Heras, J., Letizia, F., Siminski, J., and Merz, K., "Spacecraft collision avoidance challenge: design and results of a machine learning competition," *Astrodynamics*, Vol. 6, No. 2, 2022, pp. 121–140. DOI: <https://doi.org/10.1007/s42064-021-0101-5>.
- [9] Caldas, F., Soares, C., Nunes, C., and Guimarães, M., "Conjunction Data Messages for space collision behave as a Poisson process," *31<sup>st</sup> European Signal Processing Conference (EUSIPCO)*, Hesinki, Finland, 2023.
- [10] Laporte, F., "JAC Software, dedicated to the analysis of conjunction messages," *SpaceOps 2014 Conference*, Pasadena, CA, US, 5-9 May 2014. DOI: <https://doi.org/10.2514/6.2014-1774>.
- [11] Laporte, F., "JAC Software, solving conjunction assessment issues," *Proceedings of the Advanced Maui Optical and Space Surveillance Technologies Conference (AMOS)*, Maui, Hawaii, US, 9-12 September 2014.



- [12] Tardioli, C., and Vasile, M., "Collision and re-entry analysis under aleatory and epistemic uncertainty," *Advances in Astronautical Sciences*, Vol. 156, 2015, pp. 4205 – 4220.
- [13] Delande, E., Houssineau, J., and Jah, M., "A New Representation of uncertainty for data fusion in SSA Detection and Tracking Problems," *2018 21st International Conference on Information Fusion (FUSION)*, Cambridge, United Kingdom, 2018. DOI: <https://doi.org/10.23919/ICIF.2018.8455540>.
- [14] Balch, M., Martin, R., and Ferson, S., "Satellite conjunction analysis and the false confidence theorem," *Proceedings of the Royal Society A: Mathematical, Physical and Engineering Sciences*, Vol. 475, No. 20180565, 2019. DOI: <https://doi.org/10.1098/rspa.2018.0565>.
- [15] Greco, C., Sánchez, L., and Vasile, M., "A robust Bayesian agent for optimal collision avoidance manoeuvre planning," *8<sup>th</sup> European Conference on Space Debris*, ESA/ESOC, Darmstadt, Germany, 12-14 April 2021.
- [16] Sánchez, L., and Vasile, M., "On the use of machine learning and evidence theory to improve collision risk management," *Acta Astronautica*, Vol. 181, 2021, pp. 694–706. DOI: <https://doi.org/10.1016/j.actaastro.2020.08.004>.
- [17] Sánchez, L., and Vasile, M., "Intelligent agent for decision-making support and collision avoidance manoeuvre design on space traffic management," *Advances in Space Research. In press*, 2022. DOI: <https://doi.org/10.1016/j.asr.2022.09.023>.
- [18] Sánchez, L., Stevenson, E., Vasile, M., Rodríguez-Fernández, V., and Camacho, D., "An intelligent system for robust decision-making in the all-vs-all conjunction screening problem," *3<sup>rd</sup> IAA Conference on Space Situational Awareness (ICSSA)*, Tres Cantos, Madrid, Spain, 4-6 April 2022.
- [19] Helton, J. C., Oberkampf, W., and Johnson, J., "Competing failure risk analysis using evidence theory," *Risk Analysis*, Vol. 25, No. 4, 2005, pp. 973–995. DOI: <https://doi.org/10.1111/j.1539-6924.2005.00644.x>.
- [20] Dvoretzky, A., Kiefer, J., and Wolfowitz, J., "Asymptotic minimax character of the sample distribution function and of the classical multinomial estimator," *Annals of Mathematical Statistics*, Vol. 27, No. 3, 1956, pp. 642–669. DOI: <https://doi.org/10.1214/aoms/1177728174>.
- [21] Shafer, G., *A Mathematical theory of evidence*, 1<sup>st</sup> ed., Princeton University Press, Princeton, NJ, 1976. ISBN: 9780691100425.
- [22] Serra, R., Arzelier, D., Joldes, M., Lasserre, J., Rondepierre, A., and Salvy, B., "Fast and accurate computation of orbital collision probability for short-term encounters," *Journal of Guidance, Control, and Dynamics*, Vol. 39, 2016, pp. 1–13. DOI: <https://doi.org/10.2514/1.G001353>.
- [23] Greco, C., and Vasile, M., "Robust Bayesian particle filter for space object tracking under severe uncertainty," *Journal of Guidance, Control, and Dynamics*, Vol. 45, No. 3, 2021, pp. 481–498. DOI: <https://doi.org/10.2514/1.G006157>.
- [24] Ferson, S. and Kreinovich, V. and Ginzburg, L. and Sentz, K. and Myers, D.S., "Constructing probability boxes and Dempster-Shafer structures," Tech. rep., Sandia National Lab., Albuquerque, NM, United States, 2023. DOI: <https://doi.org/10.2172/809606>.

- [25] Ferson, S., Kreinovich, V., Hajagos, J., Oberkampf, W., and Ginzburg, L., *Experimental uncertainty estimation and statistics for data having interval uncertainty*, Princeton University Press, Sandia National Laboratories (SNL), Albuquerque, NM, and Livermore, CA (United States), 2007, Chap. 4: Descriptive statistics for interval data, pp. 28–87. DOI: <https://doi.org/10.2172/910198>.
- [26] He, Y., Mirzargar, M., and Kirby, R., “An efficient reliability analysis approach for structure based on probability and probability box models,” *Structural and Multidisciplinary Optimization*, Vol. 56, 2017, pp. 167–181. DOI: <https://doi.org/10.1007/s00158-017-1659-7>.
- [27] European Space Agency, “Kelvins collision avoidance challenge,” <https://kelvins.esa.int/collision-avoidance-challenge/home/>, 2019.
- [28] He, Y., Mirzargar, M., and Kirby, R., “Mixed aleatory and epistemic uncertainty quantification using fuzzy set theory,” *International Journal of Approximate Reasoning*, Vol. 66, 2015, pp. 1–15. DOI: <https://doi.org/10.1016/j.ijar.2015.07.002>.
- [29] Chojnacki, E., Baccou, J., and Destercke, D., “Numerical sensitivity and efficiency in the treatment of epistemic and aleatory uncertainty,” *5<sup>th</sup> International Conference on Sensitivity Analysis of Model Output*, Budapest, Hungary, 18-22 June 2007. DOI: <https://doi.org/10.1016/j.ijar.2015.07.002>.
- [30] Ferson, S., Nelsen, R., Hajagos, J., Berleant, D., Zhang, J., Tucker, W. T., Ginzburg, L. R., and Oberkampf, W., “Dependence in probabilistic modeling, Dempster-Shafer theory, and probability bounds analysis,” Tech. rep., Sandia National Lab., United States, Oct. 2004. DOI: <https://doi.org/10.2172/919189>.
- [31] Stroe, I., Stanculescu, A., Iliaica, P., Blaj, C., Nita, M., Butu, A., Escobar, D., Tirado, J., Bija, B., and Saez, D., “AUTOCA autonomous collision avoidance system,” *8<sup>th</sup> European Conference on Space Debris*, ESA/ESOC, Darmstadt, Germany, 20-23 April 2021.